REPORT DOCUMENTATION PAGE

Form Approved
OMB No. 0704-0188

PLEASE DO NOT RETURN YOUR FORM TO THE ABOVE ADDRESS.

1. REPORT DATE *(DD-MM-YYYY)*	2. REPORT TYPE	3. DATES COVERED *(From - To)*
22-05-2001	Final	15-05-1998 -- 31-12-2000

4. TITLE AND SUBTITLE

Design and Analysis Methods for Equipment Emulation in the Shock Qualification of Deck Structures

5a. CONTRACT NUMBER
N00014-98-1-0755

5b. GRANT NUMBER
98PR06526-00

5c. PROGRAM ELEMENT NUMBER

6. AUTHOR(S)

Dupont, Pierre, E.

5d. PROJECT NUMBER

5e. TASK NUMBER

5f. WORK UNIT NUMBER

7. PERFORMING ORGANIZATION NAME(S) AND ADDRESS(ES)

Trustees of Boston University
Office of Sponsored Programs
881 Commonwealth Ave.
Boston, MA 02215

8. PERFORMING ORGANIZATION REPORT NUMBER

9. SPONSORING/MONITORING AGENCY NAME(S) AND ADDRESS(ES)

Office of Naval Research
Program Officer Dr. Luise Couchman ONR 334
Ballston Centre Tower One
800 North Quincy Street
Arlington, VA 22217-5660

10. SPONSOR/MONITOR'S ACRONYM(S)

11. SPONSORING/MONITORING AGENCY REPORT NUMBER

12. DISTRIBUTION AVAILABILITY STATEMENT

Approved for public release; distribution is unlimited.

20010525 076

13. SUPPLEMENTARY NOTES

14. ABSTRACT

An important goal in the design of many large structures, such as ships and buildings, is the isolation of attached equipment from shock and vibration loads. Due to the high fabrication cost of such structures, extensive dynamic analysis of design concepts is carried out using finite element models and scaled mechanical models. The validity of such testing depends on the fidelity of the models employed. The finite element codes and scale modeling techniques currently in use, however, do not always achieve the requisite level of fidelity. This research project focused on the creation of analytical tools for the design of efficient, high-accuracy structural models. Two specific examples were studied in this research: (1) the modeling of distributed damping materials and (2) the design of mechanical emulators for modally dense equipment.

15. SUBJECT TERMS

shock, vibration, damping models, equipment emulators, model reduction.

16. SECURITY CLASSIFICATION OF:			17. LIMITATION OF ABSTRACT	18. NUMBER OF PAGES	19a. NAME OF RESPONSIBLE PERSON
a. REPORT	b. ABSTRACT	c. THIS PAGE			Pierre E. Dupont, Associate Professsor
U	U	U	UU	53	19b. TELEPONE NUMBER *(Include area code)* 617-353-9596

Final Report

Principal Investigator:	Pierre E. Dupont
Organization:	Boston University
Address:	Aerospace and Mechanical Engineering Boston, MA 02215

Contract / Grant Number:	N00014-98-1-0755
PR Number	98PR06526-00
Contract / Grant Title:	Design and analysis Methods for Equipment Emulation in the Shock Qualification of Deck Structures
Program Officer:	Dr. Luise Couchman

Contents

Research Objectives

An important goal in the design of many large structures, such as ships and buildings, is the isolation of attached equipment from shock and vibration loads. Due to the high fabrication cost of such structures, extensive dynamic analysis of design concepts is carried out using finite element models and scaled mechanical models. The validity of such testing depends on the fidelity of the models employed. The finite element codes and scale modeling techniques currently in use, however, do not always achieve the requisite level of fidelity. The objective of this research was the creation of analytical tools for the design of efficient, high-accuracy structural models. Two specific examples studied in this research were (1) the modeling of distributed damping materials and (2) the design of mechanical emulators for modally dense equipment.

Modeling Distributed Damping

To improve the models of damping treatments in finite element codes, a wave-based method was developed to estimate frequency-dependent structural damping in shock-loaded structures. Working with Dr. Liming Salvino of the Naval Surface Warfare Center, Carderock Division, this approach was applied successfully to the estimation of damping in box beams filled with granular material. This work addressed two goals of the original proposal – the design of experimental methods for shock testing and the assessment of damping effectiveness during shock loading. These results have been published in the Journal of Sound and Vibration.

Design of Equipment Emulators

Equipment emulators are mechanical scale models that approximate the input-output dynamic behavior of the full-scale equipment where it attaches to its foundation. This behavior can be described by an impedance matrix associated with the foundation attachment locations. Note that since for a wide range of loading conditions, equipment behavior is linear, the scaling itself is not a research issue. Rather the fundamental problem is the complicated designs of the full-scale equipment, which cannot simply be miniaturized. Thus, the design problem involves trading off emulator complexity (and so cost) with input-output error. The design process can be decomposed into the following three steps:

- Experimental modeling of actual equipment – A frequency domain input-output model of the full-scale equipment is obtained by applying forces at the locations where it attaches to its foundation and measuring the resulting velocity at these locations.
- Model reduction – In this step, the experimental model is approximated analytically and its complexity is then reduced to an acceptable level at the cost of increasing modeling error.
- Mechanical realization – Once a simplified frequency-domain model is obtained, it must be built. The mechanical realization problem is to derive a mechanical design from the frequency domain model.

During the period of this grant, the focus was on identifying model reduction techniques for modally dense equipment.

Technical Approach

Modeling Distributed Damping

There are many situations in which constitutive models of special materials are unknown and the research to obtain such a model is deemed too costly. In these cases, a phenomenological model can often be derived from experiment at modest cost. These phenomenological models can then be applied to simulating the behavior of systems under conditions similar to those for which the model was derived. When considering the effect of damping treatments under conditions of shock loading, however, this approach is complicated by the fact that widely used time-domain finite element codes, such as *LS-DYNA* and *VIBES*, only allow the user to specify Rayleigh damping. The Rayleigh damping matrix is given by a weighted sum of the mass and stiffness matrices and so is not appropriate for expressing general frequency dependent damping behavior.

To remedy this deficiency without necessitating a rewriting of the codes, an approach was developed in which distributed damping treatments are represented as an array of discrete attachments located at the model elements' nodes. This approach, referred to as *inverse homogenization,* is an excellent approximation at low frequencies, and so is applicable to shock response. For a particular damping treatment, the steps involved in developing the phenomenological model are as follows.

1. Solve for the material properties of the untreated structure. This can be done by comparing the experimental and finite element model responses of the base structure.
2. Solve for a frequency domain discretized model of the damping treatment. In this step, an optimization technique is used to match the experimental response of the damped structure with a finite element model of the base structure with an array of frequency-dependent attached impedances.
3. Obtain a time-domain model of the array impedance. A state space model of the impedance is derived and implemented as a subroutine that computes a damping force based on its current state and velocity.

This methodology was developed in the context of granular fill damping in box beams.

Design of Equipment Emulators

Toward the development of a design approach for scale models, techniques for producing reduced order models have been investigated. These techniques would allow a designer to specify model complexity (and thus cost) as well as permissible modeling error. The approach taken has been to examine model reduction techniques based on truncation of a state space model, where the latter is defined as follows.

$$\begin{aligned} \dot{x} &= Ax + Bu \\ y &= Cx + Du \end{aligned}, \quad \begin{aligned} &x \in \mathbb{R}^n, \text{ vector of } n \text{ states}, \quad m \ll n \\ &u \in \mathbb{R}^m, \text{ vector of } m \text{ attachment points velocities} \\ &y \in \mathbb{R}^m, \text{ vector of } m \text{ attachment points forces} \end{aligned} \tag{1}$$

The state space model is related to the admittance transfer function $G(j\omega)$ by

$$G(j\omega) = C\left(j\omega I - A\right)^{-1} B + D \tag{2}$$

In state space truncation, the model of (1) is partitioned and truncated as shown below

$$\begin{aligned} \left[\begin{array}{c} \dot{x}_1 \\ \hline \dot{x}_2 \end{array}\right] &= \left[\begin{array}{c|c} A_{11} & A_{12} \\ \hline A_{21} & A_{22} \end{array}\right]\left[\begin{array}{c} x_1 \\ \hline x_2 \end{array}\right] + \left[\begin{array}{c} B_1 \\ \hline B_2 \end{array}\right] u \qquad \begin{array}{l} x_1 \in \mathbb{R}^r \\ x_2 \in \mathbb{R}^{n-r} \end{array} \\ y &= \left[C_1 \mid C_2\right] x + Du \end{aligned} \tag{3}$$

The resulting reduced order model is given by

$$\begin{aligned} \dot{x}_1 &= A_{11} x_1 + B_1 u \\ y &= C_1 x_1 + Du \end{aligned}, \quad \left(A_{11}, B_1, C_1, D\right) \approx \hat{G}(jw) \tag{4}$$

and the error introduced by truncation is described by

$$\text{Error} = \left\| G(jw) - \hat{G}(jw) \right\| \tag{5}$$

The goal is to find the state space coordinates x, which introduce the least error for a reduced model of order r. Three techniques were considered:

1. Modal truncation – states are selected based on physical analogy.
2. Balanced truncation – states are selected based on their contribution to energy transfer.
3. Balanced stochastic truncation – states are selected based on their contribution to phase matching.

Research on the mechanical realization problem was also initiated during this period. The following four approaches to obtaining a mechanical scale model given a reduced order transfer function $\hat{G}(j\omega)$ were considered.

1. Transform directly to modal coordinates – The motivation here is that the mechanical system is obvious once the modal coordinates are given.
2. Employ numerical approximation – In this approach, a feasible mechanical model set is defined and the member of that set is selected by numerically minimizing the error criteria given by (5).
3. Adapt electrical network synthesis theory – This is the electrical analogue of mechanical realization, which has been developed to implement passive transfer functions as RLC circuits.

Review of Progress and Accomplishments

Modeling Distributed Damping

This research was carried out using experimental data provided by Dr. Liming Salvino of the Naval Surface Warfare Center, Carderock Division. The data consisted of acceleration measurements taken along the length of a box beam filled with granular damping material and excited by a transverse hammer blow at one end. During the period of this grant, steps 1 and 2 of the modeling process were completed. Namely, the material properties of the empty beam have been identified and a discretized frequency domain model of the fill material has been estimated. These results are discussed below.

A schematic of the beam appears in Figure 1. The equation describing its response is given by

$$\frac{EI}{i\omega}\frac{d^4v}{dx^4}+\omega\rho Av=F(\omega)\delta(x)-Z(\omega)\sum_{n=1}^{N}\delta(x-x_n)v \tag{6}$$

This is the usual beam equation in which v describes the vertical deflection, x describes the distance along the beam and F is the forcing due to the hammer blow. If the last term on the right side is neglected, the same equation governs the empty beam response.

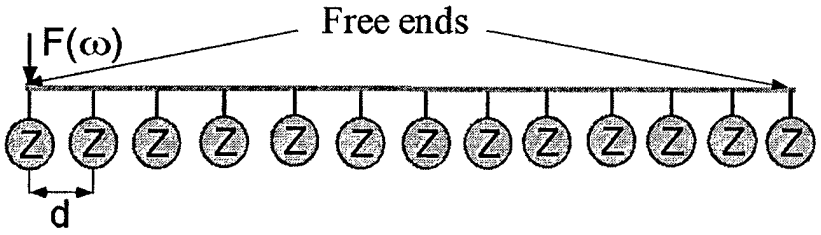

Figure 1. Schematic of beam with discretized attachments of impedance Z.

By minimizing the error function of (7) subject to the passivity constraint of (8), a frequency domain model of Z has been obtained which accurately reproduces the experimental data.

$$Error=\sum_{n=1}^{N}\frac{\left|v_n^{(\text{fem})}-v_n^{(\text{data})}\right|^2}{\left|\left(v_n^{(\text{data})}\right)^2\right|} \tag{7}$$

$$\text{Re}\{Z(\omega)\}\geq 0 \tag{8}$$

An example of the excellent response matching in both the frequency and time domains is depicted in Figure 2. Note that the discrete model was obtained from one experimental trial and then used to simulate a second trial for the comparison shown.

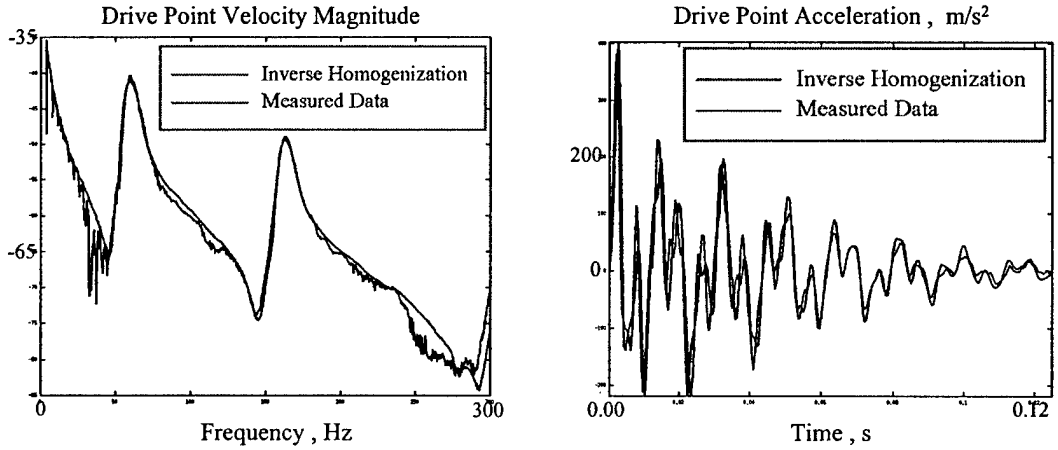

Figure 2. Example comparing discretized model with filled beam response.

As identified, the impedance model for Z is estimated at discrete frequencies. A rational function approximation of the form given by (9) is needed. This can be obtained using maximum likelihood approximation.

$$Z(\omega) \approx Z_{\text{rational}}(\omega) = \frac{a_0 + a_1\omega + \ldots + a_M\omega^M}{b_0 + b_1\omega + \ldots + b_N\omega^N} \tag{9}$$

An example using this approach is shown in Figure 3.

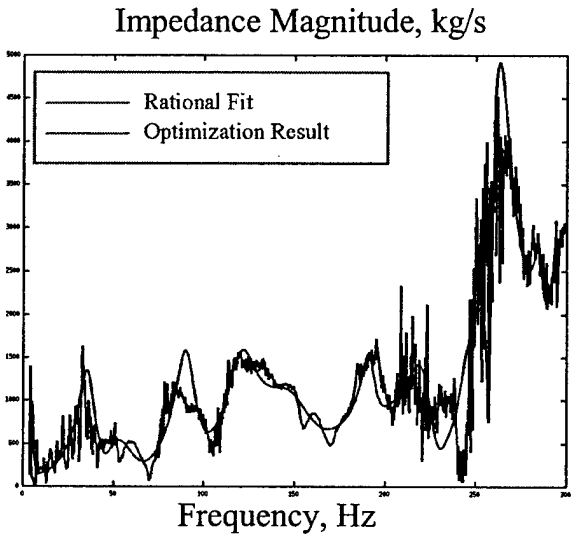

Figure 3. Rational function approximation to granular fill impedance.

Design of Equipment Emulators

Model reduction techniques were compared for single input, single output systems of high modal density. An example system is depicted in Figure 4. The base mass represents the main structure while the multi-mass subsystem on top represents the equipment. Our results verified that modal truncation is equivalent to balanced truncation when the modes are widely spaced and lightly damped. It was also demonstrated that balanced truncation does not guarantee preservation of model passivity. This means that, while the actual equipment can only store or dissipate vibrational energy, a nondissipative reduced model is capable of generating vibrational energy – a nonphysical result. Balanced stochastic truncation guarantees preservation of passivity and typically gave the smallest model reduction error. An example for the system of Figure 4 appears in Figure 5.

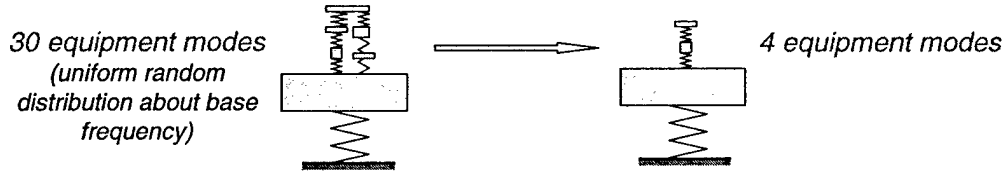

Figure 4. Example of single input, single output model reduction.

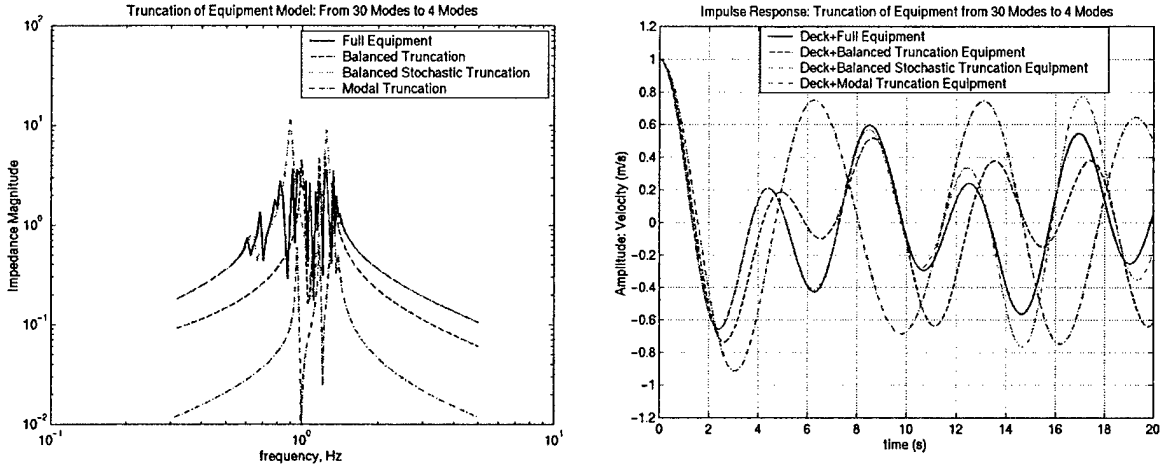

Figure 5. Impedance magnitude and impulse response of modal, balanced and balanced stochastic truncation.

Three potential approaches to the mechanical realization problem were investigated. This problem is to solve for a mechanical system that matches the dynamic behavior of the reduced order model. The first approach considered was to attempt to transform the reduced model to modal coordinates. Even though the full-order system could be expressed in modal coordinates, it was demonstrated that truncation in either balanced or balanced stochastic coordinates did not permit transformation back to modal coordinates. Since truncation in modal coordinates was found to be inferior for modally dense systems, this approach was abandoned. These results did suggest the idea of developing a model reduction approach that preserves the underlying mechanical system equation structure. This approach and numerical approximation are

considered the most promising approaches for future work. Electrical network synthesis theory was also studied and found to be of limited practical value for mechanical realization.

Relevance to the Navy

The spatial wave damping estimation technique developed in this research is of great interest to the Navy. The PI has worked with Dr. Liming Salvino of NSWC, Carderock, to apply the technique to the estimation of damping provided by granular fill materials in box beams. In contrast to traditional modal approaches that provide estimates only at modal frequencies of the test structure, this technique estimates damping over a broad range of frequencies. The approach can be used to incorporate phenomenological damping models in time-domain finite element codes. This technique will be of interest to Naval contractors. In particular, technical discussions were held with ETC personnel.

Scaled testing of ship structures is used to assess the acoustic and shock isolation afforded by deck and mount designs. Techniques for designing equipment models with specified error bounds are of direct use to navy engineers. The results of this research have been presented to Dr. Vern Simmons and Mr. William Martin of NSWC, Carderock, who are keenly interested in emulator technology for use in future advanced structures programs.

List of Publications and Presentations

Refereed Papers

1. "A Wave Approach to Measuring Frequency-dependent Damping Under Transient Loading," J.G. McDaniel, P. Dupont and L. Salvino, *Journal of Sound and Vibration*, Vol. 231, No. 2, 23 March 2000, pp. 433-449.

2. "Evaluation of Granular-fill Damping in Shock Loaded Box Beams," L. Salvino, P. Dupont and J.G. McDaniel, *Proceedings of the 69th Shock and Vibration Symposium*, St. Paul, MN, October 1998.

3. "Model Reduction Techniques for Shock Loaded Equipment Emulators," P. Dupont and A. Stokes, *Proceedings of the 69th Shock and Vibration Symposium*, St. Paul, MN, October 1998.

Non-Refereed Papers

1. "An Error Measure for the Shock Testing of Scale Models," P. Dupont and J.G. McDaniel, *16th International Conference on Acoustics and 135th Meeting of the Acoustical Society of America*, Seattle, WA, June 1998.

2. "A Wave Approach to Measuring Frequency-dependent Damping Under Transient Loading," J.G. McDaniel, P. Dupont and L. Salvino, Boston University, Aerospace and Mechanical Engineering Technical Report No. AM-99-009.

Invited Presentation

1. P. Dupont and J. McDaniel, "Assessing Damping Efficacy of Granular Fills in Shock Loaded Box Beams," Advanced Machinery Support System Shock Meeting, Naval Surface Warfare Center, Carderock Division, Bethesda, MD, 18 May 1998.

Contributed Presentations

1. "Shock Error and Sensitivity Measures for Equipment Emulators," P. Dupont, J.G. McDaniel and A. Stokes, 69th Shock and Vibration Symposium, St. Paul, MN, October 1998.

2. "Evaluation of Granular-fill Damping in Shock Loaded Box Beams," L. Salvino, P. Dupont and J.G. McDaniel, 69th Shock and Vibration Symposium, St. Paul, MN, October 1998.

3. "An Error Measure for the Shock Testing of Scale Models," P. Dupont and J.G. McDaniel, 16th International Conference on Acoustics and 135th Meeting of the Acoustical Society of America, Seattle, WA, June 1998.

Reprinted Papers

This section contains reprints of the following publications.

1. "A Wave Approach to Measuring Frequency-dependent Damping Under Transient Loading," J.G. McDaniel, P. Dupont and L. Salvino, *Journal of Sound and Vibration*, Vol. 231, No. 2, 23 March 2000, pp. 433-449.

2. "Evaluation of Granular-fill Damping in Shock Loaded Box Beams," L. Salvino, P. Dupont and J.G. McDaniel, *Proceedings of the 69th Shock and Vibration Symposium*, St. Paul, MN, October 1998.

3. "Model Reduction Techniques for Shock Loaded Equipment Emulators," P. Dupont and A. Stokes, *Proceedings of the 69th Shock and Vibration Symposium*, St. Paul, MN, October 1998.

4. "An Error Measure for the Shock Testing of Scale Models," P. Dupont and J.G. McDaniel, 16th International Conference on Acoustics and 135th Meeting of the Acoustical Society of America, Seattle, WA, June 1998

A Wave Approach to Measuring Frequency-dependent Damping Under Transient Loading

J.G. McDaniel, P. Dupont and L. Salvino, *Journal of Sound and Vibration*, Vol. 231, No. 2, 23 March 2000, pp. 433-449.

A Wave Approach to Estimating Frequency-dependent Damping Under Transient Loading*

J. Gregory McDaniel and Pierre Dupont
Aerospace & Mechanical Engineering
Boston University
Boston, MA 02215

Liming Salvino
Naval Surface Warfare Center, Carderock Division
West Bethesda, MD 20817

Abstract

A wave model is proposed for estimating damping loss factor as a function of frequency for a beam with arbitrary transient loading applied through the boundary conditions. In contrast to modal methods which provide measures of damping only at the modal frequencies of the test structure, the damping factor is determined over discrete, but regularly-spaced, frequency values associated with the temporal sampling frequency. This makes it possible to predict or simulate damping in complex structures built from the tested component. Numerical and experimental data from a free-free beam are used to validate the approach.

1 Introduction

A new method is presented for estimating the frequency-dependent loss factor of a damped vibrating beam from its transient response measured at several locations. The method, which is applied here to numerical and experimental beam data, uses the Fourier transform of the measured transient responses. Knowledge of the beam's equation of motion is used to express the transformed responses at any frequency as a sum of four damped waves. The loss factor is a simple function of the spatial decays of these waves and may be estimated at any frequency for which the Fourier transform can be accurately obtained. For short-time excitations, this method allows one to estimate the loss factor at many frequencies, thus overcoming the inherent limitations of modal descriptions that only estimate the loss factor at the natural frequencies of the structure.

* *Journal of Sound and Vibration*, Volume 231(2), 23 March 2000, pages 433-449.

In recent years, a number of authors have developed representations of structural response in terms of damped waves described by complex wavenumbers. For example, Plona *et al.* presented theoretical and experimental studies of the complex wavenumbers of axisymmetric waves propagating in cylindrical shells in contact with various acoustic media [1]. Their experimental results were generated by exciting the shell with one cycle sinewave bursts centered at the frequency of interest. Vollman *et al.* studied the complex wavenumbers of up to 40 waves propagating in a cylindrical shell in contact with a viscoelastic medium [2]. Their work, which also presented theoretical and experimental results, used a complex spectrum estimation technique. McDaniel *et al.* demonstrated that the complex wavenumbers, amplitudes, and loss factor of a mechanically excited damped beam could be determined from a small array of accelerometers at any frequency of excitation [3]. Their approach used an iterative scheme that minimized the error between the wave description and the measured responses by adjusting the complex wavenumbers and amplitudes.

The problem addressed here is significantly different than those mentioned above in that the excitation occurs over a very short time period. Consequently, the structure is in free vibration for most of this period. Because free response is composed only of the natural modes of the system, it was not clear *a priori* that wave phenomenon at non-resonant frequencies would be observed. Furthermore, a mathematical formulation did not exist for expecting that the Fourier transform of the the beam's response would be composed of only a sum of waves at any frequency. This formulation is presented here and indicates that if the structure has zero initial conditions and the Fourier transform is taken over a sufficiently large time window, such that the response has decayed, then the responses at any transform frequency may be represented as a sum of waves. Furthermore, the numerical and experimental results support the hypothesis that damping can be estimated over a broad frequency range using an excitation of short duration.

This work was motivated by the need to assess damping in shock-loaded truss structures composed of many box beams filled with small viscoelastic beads. Phillips [4] recently presented experimental results of such a truss and found that the beads substantially increased the damping of the truss. One way of investigating the vibrational characteristics of many truss designs, as well as their interactions with attached structures, without fabricating them is to construct and interrogate finite element models. However, the loss factor associated with each beam is difficult to estimate, as it depends on the details, such as bead sizes and their dynamic interactions. This difficulty is overcome by performing experiments on one section of a beam and using the experimental data to estimate the loss factor in the band of interest. Because the loss factor of a filled beam is known to be a strong function of frequency, as experimentally demonstrated by House [5], we desire loss factor estimates at many frequencies in the band. These estimates are made possible by the method described here.

Section 2 presents the theoretical foundation for the method. Expressions for wave and modal estimates of the loss factor are derived. The transient response is expressed as a sum of a wave solution and a modal solution. Because the initial conditions are zero for a shock event, the modal solution is identically zero and the Fourier transform of the transient response may, at each frequency, be written as a sum of four damped waves. Once the

forcing has ended, however, a transient modal solution can be obtained. In section 3, the wave model is applied to a finite element beam model as well as actual beam data. Using the finite element model, the frequency bounds of the loss factor estimation procedure are investigated. The results are then applied to the analysis of a bead-filled box beam and a comparison is made to modal damping estimates. The paper concludes with guidelines for use of the method.

2 Damping Theory

In developing the solution for the forced response, the premise of this paper is that the total solution, $y(x,t)$ can be written as a sum of wave and modal solutions.

$$y(x,t) = y_w(x,t) + y_m(x,t) \tag{1}$$

Here, y_w represents the wave solution which is required to satisfy homogeneous initial conditions and nonhomogeneous boundary conditions. The modal solution, y_m, is required to satisfy nonhomogeneous initial conditions and homogeneous boundary conditions. In other words, the modal solution accounts for nonzero initial conditions, $y(x, t = 0)$ and the wave solution accounts for forcing terms appearing in the boundary conditions.

The differential equation which both the modal and wave solutions must satisfy is given by

$$\rho\frac{d^2y}{dt^2} + \mathcal{L}\{y\} = 0 \tag{2}$$

where $\mathcal{L}$ is a time invariant linear operator involving derivatives with respect to x. It is subject to boundary conditions of the form

$$\mathcal{L}_b\{y\}|_{x=x_b} = \begin{cases} f(t), & \text{wave solution} \\ 0, & \text{modal solution} \end{cases} \tag{3}$$

in which $x_b = \{0, L\}$ and $\mathcal{L}_b$ is time-invariant and involves spatial derivatives of y. The boundary forcing is such that $f(t < 0) = 0$ and $\lim_{t\to\infty} f(t) = 0$.

The modal response to nonzero initial conditions is the approach commonly employed in modeling transient response data. Only the wave solution due to transient forcing will be developed here. In particular, the equations will be presented in the context of a free-free beam excited by a shear force at one end.

2.1 Wave Solution

The form of (2) describing a free-free beam is

$$m\frac{\partial^2 y_w}{\partial t^2} + EI\frac{\partial^4 y_w}{\partial x^4} = 0 \tag{4}$$

Homogeneous initial conditions are assumed:

$$y_w(x, t=0) = 0 \tag{5}$$
$$\dot{y}_w(x, t=0) = 0 \tag{6}$$

The boundary conditions of (3) are given by

$$\begin{aligned} M(x=0,t) &= EI\frac{\partial^2 y_w}{\partial x^2}\Big|_{x=0} &&= 0 \\ Q(x=0,t) &= -EI\frac{\partial^3 y_w}{\partial x^3}\Big|_{x=0} &&= f(t) \\ M(x=L,t) &= EI\frac{\partial^2 y_w}{\partial x^2}\Big|_{x=0} &&= 0 \\ Q(x=L,t) &= -EI\frac{\partial^3 y_w}{\partial x^3}\Big|_{x=0} &&= 0 \end{aligned} \tag{7}$$

Equations (4) and (7) will be transformed with respect to time using the Fourier transform pair

$$G(\omega) = \frac{1}{2\pi}\int_{-\infty}^{\infty} g(t)e^{i\omega t}dt, \quad g(t) = \int_{-\infty}^{\infty} G(\omega)e^{-i\omega t}d\omega \tag{8}$$

Employing the homogeneous initial conditions of (5)and assuming that $\lim_{t\to\infty} y_w(t) = 0$, the transformed beam equation (4) is given by

$$E(1 - i\eta(\omega))I\frac{\partial^4 Y_w(x,\omega)}{\partial x^4} - \omega^2 m Y_w(x,\omega) = 0 \tag{9}$$

where damping has been introduced in the frequency domain through a complex modulus of elasticity, $E(1 - i\eta(\omega))$.

The solution of this homogeneous equation is of the form

$$Y_w(x,\omega) = c_1(\omega)e^{ikx} + c_2(\omega)e^{-ikx} + c_3(\omega)e^{kx} + c_4(\omega)e^{-kx} \tag{10}$$

where

$$k = \sqrt[1/4]{\frac{\omega^2 m}{E(1 - i\eta(\omega))I}} \tag{11}$$

is complex due to damping. The first two terms correspond to flexural waves propagating from each end of the beam. The latter two terms correspond to evanescent waves decaying from each end of the beam. Damping causes the flexural waves to decay, and the evanescent waves to oscillate, along the length of the beam.

The complex constants $c_1(\omega)$ through $c_4(\omega)$ are obtained by forcing (10) to satisfy the transformed nonhomogeneous boundary conditions (7). The following set of simultaneous algebraic equations results when the complex modulus is inserted in the transformed boundary conditions.

$$\begin{bmatrix} (ik)^2 & (-ik)^2 & (k)^2 & (-k)^2 \\ (ik)^3 & (-ik)^3 & (k)^3 & (-k)^3 \\ (ik)^2e^{ikL} & (-ik)^2e^{-ikL} & (k)^2e^{kL} & (-k)^2e^{-kL} \\ (ik)^3e^{ikL} & (-ik)^3e^{-ikL} & (k)^3e^{kL} & (-k)^3e^{-kL} \end{bmatrix} \begin{bmatrix} c_1 \\ c_2 \\ c_3 \\ c_4 \end{bmatrix} = \begin{bmatrix} 0 \\ \frac{-F(\omega)}{E(1-i\eta(\omega))I} \\ 0 \\ 0 \end{bmatrix} \tag{12}$$

When the right-hand side and k are known, this equation can be solved at each frequency for the wave magnitudes $c_1(\omega)$ through $c_4(\omega)$. To obtain a nontrivial solution to (12), a nonzero right-hand side is the only requirement. Thus, the wave formulation presented can be applied to systems with arbitrary, albeit nonzero, boundary conditions.

The inverse transform yields the time domain solution as

$$y_w(x,t) = \int_{-\infty}^{\infty} \left(c_1 e^{ikx} + c_2 e^{-ikx} + c_3 e^{kx} + c_4 e^{-kx}\right) e^{-i\omega t} d\omega \tag{13}$$

2.1.1 Experimental Estimation of Damping

Given zero initial conditions and forcing only at the boundaries, damping can be estimated using (10) when the spatial response is known at n discrete locations, x_i, $i = 1, \ldots, n$ along the beam. In this case, a system of n nonlinear complex algebraic equations can be written at each frequency ω.

$$\begin{bmatrix} Y_w(x_1,\omega) \\ Y_w(x_2,\omega) \\ \vdots \\ Y_w(x_n,\omega) \end{bmatrix} = \begin{bmatrix} e^{ikx_1}, & e^{-ikx_1}, & e^{kx_1}, & e^{-kx_1} \\ e^{ikx_2}, & e^{-ikx_2}, & e^{kx_2}, & e^{-kx_2} \\ \vdots & \vdots & \vdots & \vdots \\ e^{ikx_n}, & e^{-ikx_n}, & e^{kx_n}, & e^{-kx_n} \end{bmatrix} \begin{bmatrix} c_1(\omega) \\ c_2(\omega) \\ c_3(\omega) \\ c_4(\omega) \end{bmatrix} \tag{14}$$

Given a guess of $k(\omega) = k_R(\omega) + ik_I(\omega)$, the wave magnitudes $c_1, \ldots, c_4$ can be estimated using linear least squares. Thus, any nonlinear optimization algorithm can be employed to find the $k(\omega)$ which minimizes an error function computed with this least squares solution. The error function used in the examples of the next section is the normalized mean square error, ϵ, defined by

$$\epsilon = \sqrt{\left(\sum_{i=1}^{n} |Y_e(x_i,\omega) - Y_a(x_i,\omega)|^2\right) / \left(\sum_{i=1}^{n} |Y_a(x_i,\omega)|^2\right)} \tag{15}$$

where $Y_e(x_i,\omega)$ and $Y_a(x_i,\omega)$ are the estimated and actual wavefields, respectively.

Given the error minimizing $k_e(\omega)$, the estimated loss factor is given by

$$\eta_e(\omega) = \left|\frac{\Im\{k_e^4\}}{\Re\{k_e^4\}}\right|, \ \omega > 0 \tag{16}$$

2.2 Modal Solution

A modal solution exists which satisfies (4), but with nonhomogeneous initial conditions

$$y_m(x, t=0) = y_0(x) \tag{17}$$
$$\dot{y}_m(x, t=0) = \dot{y}_0(x) \tag{18}$$

and homogeneous boundary conditions given by

$$\begin{aligned} M(x=0,t) &= EI\frac{\partial^2 y_m}{\partial x^2}\Big|_{x=0} = 0 \\ Q(x=0,t) &= -EI\frac{\partial^3 y_m}{\partial x^3}\Big|_{x=0} = 0 \\ M(x=L,t) &= EI\frac{\partial^2 y_m}{\partial x^2}\Big|_{x=0} = 0 \\ Q(x=L,t) &= -EI\frac{\partial^3 y_m}{\partial x^3}\Big|_{x=0} = 0 \end{aligned} \tag{19}$$

The modal solution takes the form

$$y_m(x,t) = \sum_{j=1}^{\infty} \Phi_j(x)\gamma_j(t) \tag{20}$$

where $\Phi_j(x)$ and $\gamma_j(t)$ must satisfy

$$\frac{\partial \Phi_j}{\partial x} + k_j^4 \Phi_j(x) = 0 \tag{21}$$
$$\ddot{\gamma}_j(t) + (1 - i\eta_j)\omega_j^2 \gamma_j(t) = 0 \tag{22}$$

and

$$k_j^4 = \rho A \omega_j^2 / EI \tag{23}$$

Recall that in the wave model, the entire complex modulus, $E(1 - i\eta)$ appears in the spatial equation (9). Here, it is factored such that the real modulus E appears in the spatial equation (21) and the complex damping factor in the temporal equation (22).

The temporal solution for the j^{th} mode takes the form

$$\gamma_j(t) = A_j e^{-i\omega_j\sqrt{1-i\eta_j}\,t} + A_j^* e^{i\omega_j\sqrt{1+i\eta_j}\,t} \tag{24}$$

where the positive value of ω_j is assumed and η is an odd function evaluated at $\eta_j = \eta(\omega_j > 0)$. A and A^* are complex conjugates that are related to the modal initial conditions by

$$\Re\{A_j\} = \gamma_j(0)/2 \tag{25}$$

$$\Im\{A_j\} = \frac{\dot{\gamma}_j(0) - \gamma_j(0)\omega_j \Im\{\sqrt{1-i\eta_j}\}}{2\omega_j \Re\{\sqrt{1-i\eta_j}\}} \tag{26}$$

Numerical techniques can be employed to fit the modal solution of (20) and (24) to transient response data. The damping factor, η, can be obtained from the complex frequencies of (24), $\omega_{cj} = \omega_j\sqrt{1 \pm i\eta_j}$ as

$$\eta_j = \left|\frac{\Im\{\omega_{cj}^2\}}{\Re\{\omega_{cj}^2\}}\right| \tag{27}$$

3 Examples

The proposed approach to modeling loss factor was tested on simulated as well as experimental data. In the simulation, a transient shear load was applied to one end of a finite element beam model. The goal of the simulation was to compare damping estimates obtained using modal and wave techniques for a system with a prescribed level of damping. The damping consisted of stiffness dependent Rayleigh damping. The remaining model properties and loading were selected to match a beam experiment which is also described here. In the experiment, a box beam was filled with granular material to enhance damping. The beam was struck transversely at one end with an instrumented sledge hammer. In this case, the actual damping is unknown. Prior experiments in which sinusoidal excitation was applied suggest that damping is strongly dependent on frequency. Simulation and experimental results are both described below.

3.1 Finite Element Beam Model

The model was composed of 12 Euler-Bernoulli cubic beam elements with the properties listed in Table 1. The moment of inertia was computed based on the cross section of the empty box beam. The mass per unit length corresponded to that of the box beam when filled with granular material. The prescribed Rayleigh damping was of the form

$$[C] = \alpha[M] + \beta[K] \tag{28}$$

with $\alpha = 0$ and so

$$\eta(\omega) = \omega\beta. \tag{29}$$

An actual hammer blow, sampled at 5 kHz, was applied as a shear force at $x = 0$. Measurements of transverse acceleration $a(x,t)$ were assumed available at 13 points positioned 40.64 *cm* apart along the beam.

Property	Value
E, elastic modulus	30×10^6 psi
I, moment of inertia	68.7 in^4
L, length	16 ft
m, mass per unit length	0.129 $slugs/ft$
α	0
β	2×10^{-4}

Table 1: Properties of finite element beam model.

To verify the presence of waves in the data, a frequency-wavenumber transform can be employed by computing a two-dimensional Fourier transform of the acceleration data, $a(x,t)$.

$$\mathcal{A}(\omega,k) = \frac{1}{(2\pi)^2}\int_0^T \int_0^L a(x,t)e^{i(kx+\omega t)}dxdt \tag{30}$$

The transform $\mathcal{A}(\omega,k)$ is maximized whenever the wavenumber and frequency (k,ω) coincide with that of a natural wave, (k_n,ω_n) as described by

$$a(x,t) = \Re\left\{Ae^{i(k_n x-\omega_n t)}\right\} \tag{31}$$

Note that (31) represents a forward going wave and so $\mathcal{A}(\omega,k)$ will be maximized for $k = -k_n < 0$.

Figure 1 depicts the frequency-wavenumber transform for a typical high-amplitude hammer hit. Rearranging (11), we obtain

$$\omega \approx \sqrt{\frac{EI}{m}}k^2, \quad \omega\beta \ll 1 \tag{32}$$

The two branches of this parabola are clearly visible in Figure 1 for $0 \leq \omega \leq 300$ Hz. The coarse spacing of the 13 accelerometers produces side lobes to the left and right of this parabola. They are particularly strong at the modal frequencies of the beam, i.e., $f = 42, 118, 228$ Hz. Note that the left branch of the parabola ($k < 0$) corresponds to the wave leaving the impacted end of the beam. The right branch ($k > 0$) corresponds to the wave reflected from the far end. Owing to damping, it can be seen that the magnitude of the reflected wave is reduced.

3.1.1 Loss Factor Estimation

The loss factor was estimated using equations (14)-(16) and the thirteen numerically-computed accelerations. To gain insight into the sensitivity of the estimation procedure, normally dis-

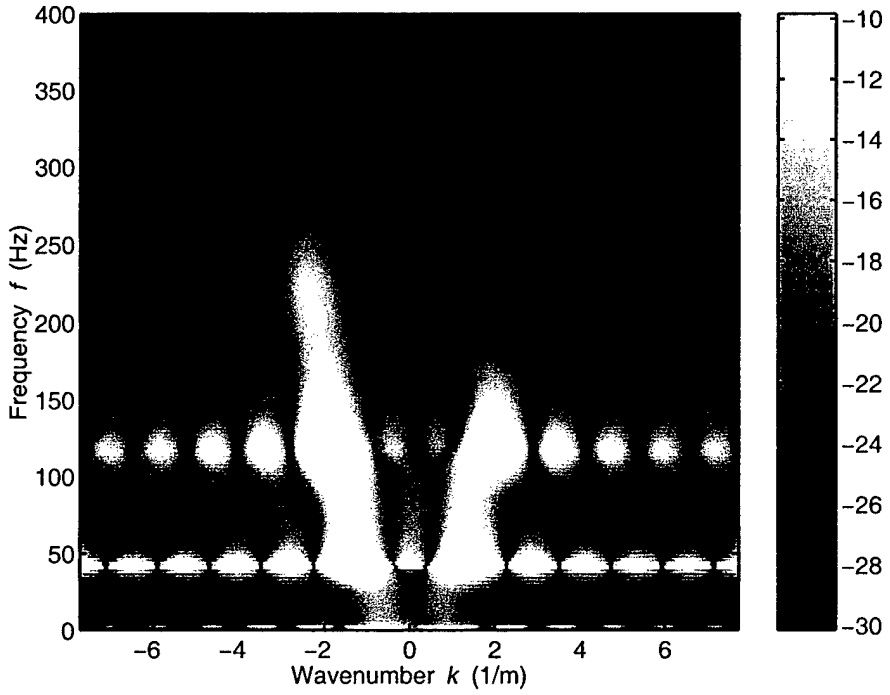

Figure 1: Frequency-wavenumber transform of finite element model acceleration response.

tributed noise with a variance of 0.98 m/s^2 (white with respect to time) was added to the acceleration data. The exact and estimated damping factors are depicted in Figure 2. Note that no attempt was made to estimate spatial damping at frequencies for which the beam length is less than half a wavelength. This is due to the weak dependence of the implemented error function on damping when evaluated over fractions of a wavelength. Thus, the abscissa starts at the first modal frequency.

Following equation (29), the exact stiffness-proportional Rayleigh damping is linear in frequency. The noise-free solution closely follows the exact solution, except for several fluctuations above 300 Hz. Similarly, agreement between the exact and noisy-data estimate is good below 300 Hz. Above 300 Hz, the estimated loss factor fluctuates widely with frequency, but with an average value approximating the exact solution. Returning to Figure 1, this result is not surprising, as it is clear that the wave energy falls off between 250 and 300 Hz.

With experimental data, the exact loss factor and signal noise are unknown. Consequently, it is worthwhile to investigate measures by which an upper frequency bound can be ascertained. A natural choice is to use the error function, ϵ, employed in the estimation procedure. Normalized mean square error, given by (15), is plotted in Figure 3. This figure confirms the observations regarding loss factor. For the noisy case, the error rapidly increases above 250 Hz. While of much smaller magnitude, the the noise-free error also increases rapidly above 250 Hz.

From Figure 1, it is clear that loss factor estimation using a wave model is only appropriate

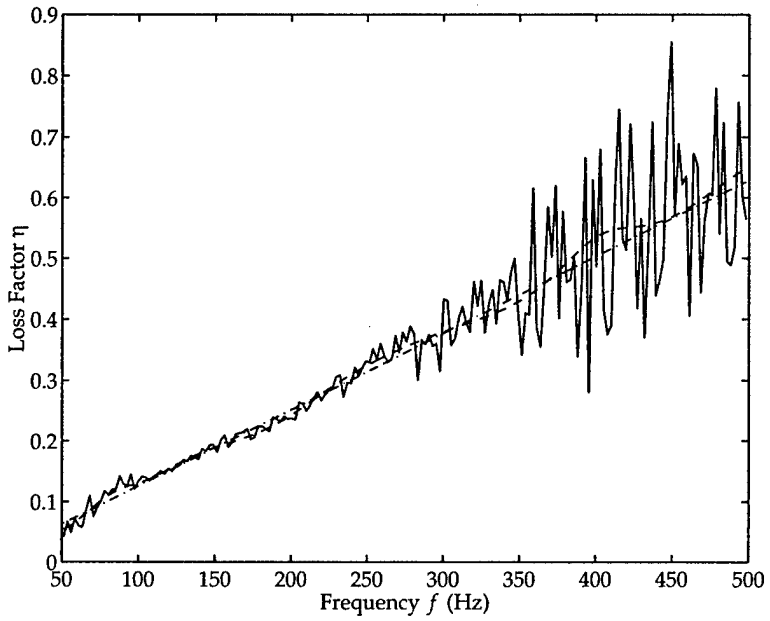

Figure 2: Loss factor versus frequency for the finite element model: $\cdot - \cdot - \cdot$, exact solution; $- - -$, estimate from noise-free simulated data; ——, estimate from noisy simulated data.

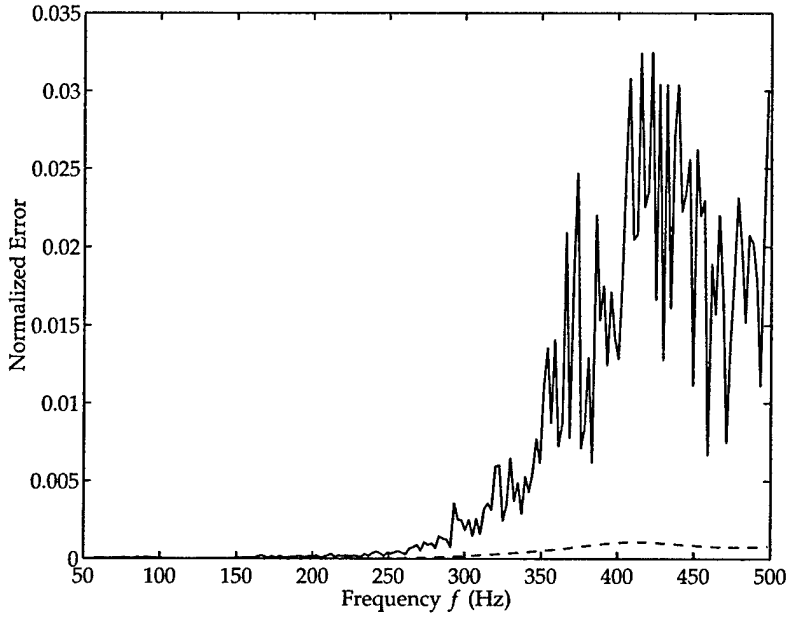

Figure 3: Normalized mean square error versus frequency for the simulated data: $- - -$, without noise; ——, with noise.

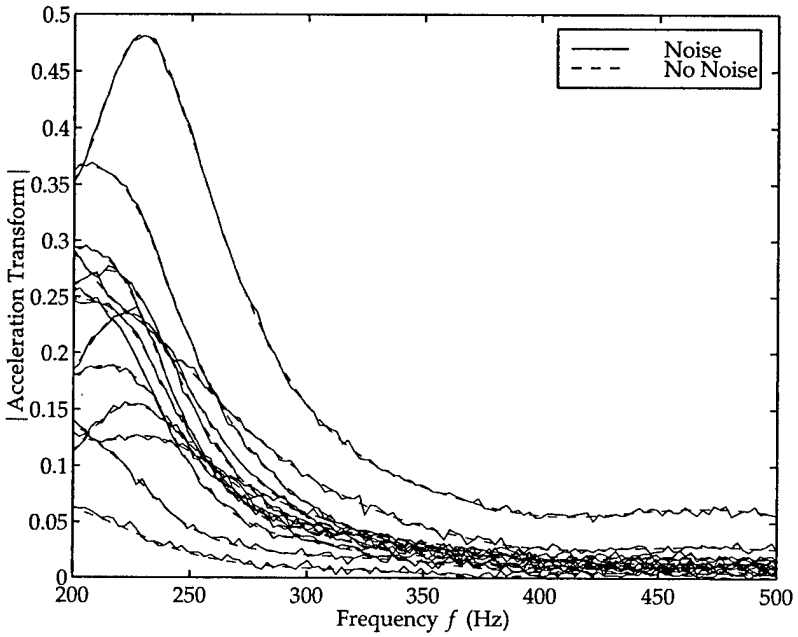

Figure 4: Magnitude of transformed acceleration versus frequency for the 13 accelerometers: – – –, without noise; ——, with noise. Note that noise dominates relative magnitudes above 250 Hz.

for frequencies at which a wave of sufficient magnitude is present in the data. Thus, the upper frequency bound for noise-free estimation is determined by the energy distribution of the impact as well as by the loss factor itself. As described in the paragraph below, the major effect of additive acceleration noise is to reduce this upper frequency bound.

Figures 1-3 clearly show that the addition of noise has a modest effect on loss factor estimation for high amplitude waves (and consequently high acceleration measurements). As frequency increases, however, wave amplitude falls off and (assuming frequency-independent noise amplitude) the noise begins to obscure the magnitude and phase relationship between the acceleration measurements along the beam. This can be seen in Figure 4 which depicts the magnitudes of the thirteen acceleration measurements used in this example. Recall from (14) that the estimation procedure involves fitting a sum of four waves to these measurements at each frequency. From 200-250 Hz, the magnitude relationship of the signals is unaffected by the noise. Above 250 Hz, however, the noise dominates the relative acceleration magnitude for many acceleration pairs.

3.2 Filled Box Beam

A steel box beam with cross section $10'' \times 6'' \times 3/8''$ and length $16'$ was suspended horizontally by elastic cords to approximate free-free boundary conditions. The beam configuration is depicted in Figure 5 and the cross section is shown in Figure 6. The elastic cords were $3/4''$ in

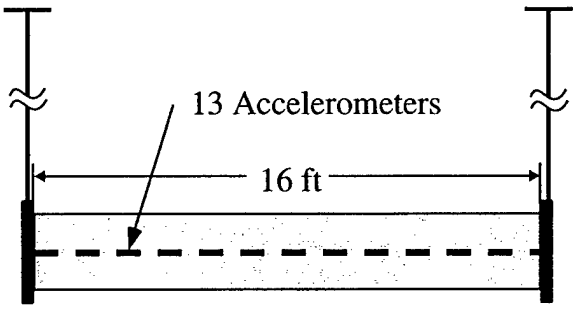

Figure 5: Beam schematic.

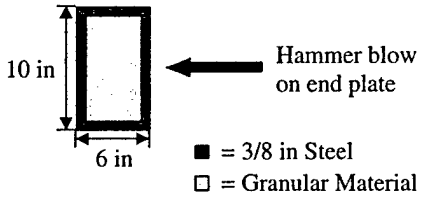

Figure 6: Beam cross section.

diameter and 20 ft in length. Steel plate endcap assemblies, with dimensions of approximately $12'' \times 8'' \times 3/4''$, were bolted to both ends of the beam for convenient installation of the fill materials. The two end plates have equal weight. With a total beam weight of approximately 603 lb., the frequencies due to the suspension are estimated at less than 5 Hz.

Chevron LDPE 1117B beads were used as the granular fill material. This material is widely used in injection molding. The weight density of the packed LDPE beads was 36.8 lbs/ft^3. The volume available to the fill material was 5.40 cubic ft. During the filling process, vibrations were applied to the beam (by tapping with a hammer) to ensure the granular material was well packed in the beam.

As shown in Figure 5, thirteen accelerometers were placed 16 inches apart on the beam along the horizontal plane passing through the center of the cross section. The number and spacing of accelerometers was chosen so as to provide approximately 6 points per wave for the 4th bending mode. The uniaxial accelerometers used in the test were calibrated to 50 g's.

3.2.1 Experimental Procedure

Flexural vibrations were excited in the horizontal plane as depicted in Figures 5 and 6. The impact forces were generated by a transverse hammer blow to one end plate on the side opposite the accelerometers. The accelerations and impact force were recorded at a sampling rate of 5 kHz using a 1 kHz low pass filter.

Ten trials of varying impact amplitude were conducted for the filled beam. The four with

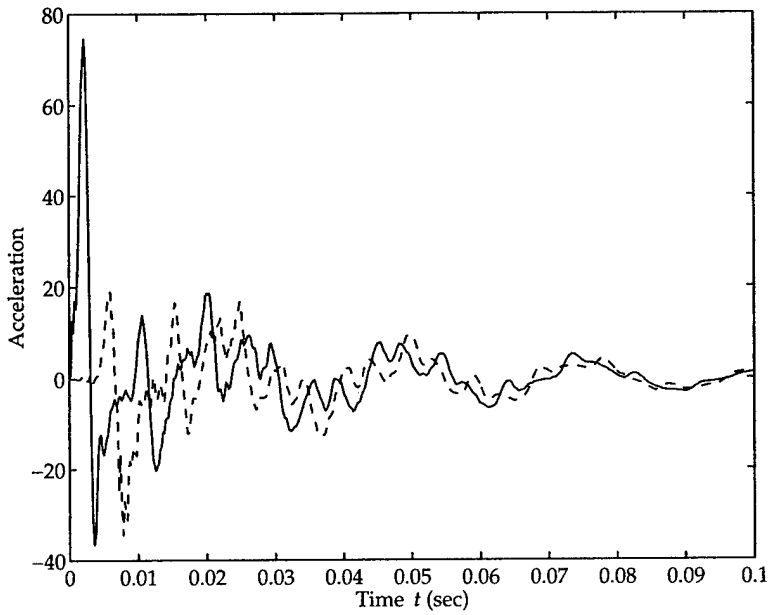

Figure 7: Acceleration (in g's) versus time at both ends of beam: ——, $x = 0$; − − −, $x = L$. Shock input was at $x = 0$.

the highest impact amplitudes were deemed to possess a sufficient signal to noise ratio up to 300 Hz to employ a wave model for loss factor estimation. For a typical trial, Figure 7 depicts the time histories of the accelerometers at the beam's impact end ($x = 0$) and far end ($x = l$). The wave speed can be deduced from the time it takes for the first peak to reach the far end of the beam. A comparison of the amplitudes of the accelerometers' first peaks demonstrates the existence of spatial damping. For $t > 0.3$ sec, the modal character of the data is apparent with the response dominated by frequencies of 37 and 108 Hz.

The Fourier transform of these acceleration histories is plotted in Figure 8. Five beam modes can be seen. The first two correspond to those observed in the time histories. A pendulum mode, due to the suspension, can also be observed at approximately 5 Hz. To verify the presence of waves in the experimental data, the frequency-wavenumber transform of (30) was employed. The result for one trial is shown in Figure 9. This figure compares favorably with the finite element model results of Figure 1.

It should be noted that box beams – empty and filled – are capable of producing plate waves which travel along the sides of the beam. Both analytical predictions and frequency wavenumber transforms of the data indicate that these waves cut on at approximately 500 Hz. Consequently, they will not be considered here.

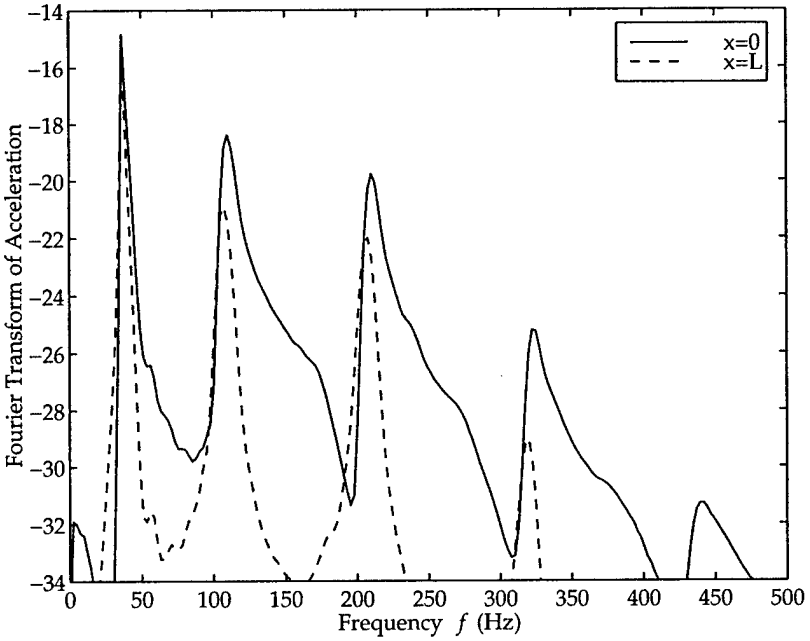

Figure 8: Acceleration versus frequency at both ends of beam: ——, $x = 0$; − − −, $x = L$. Shock input was at $x = 0$. Five highest peaks correspond to beam modes. 5 Hz peak is suspension frequency.

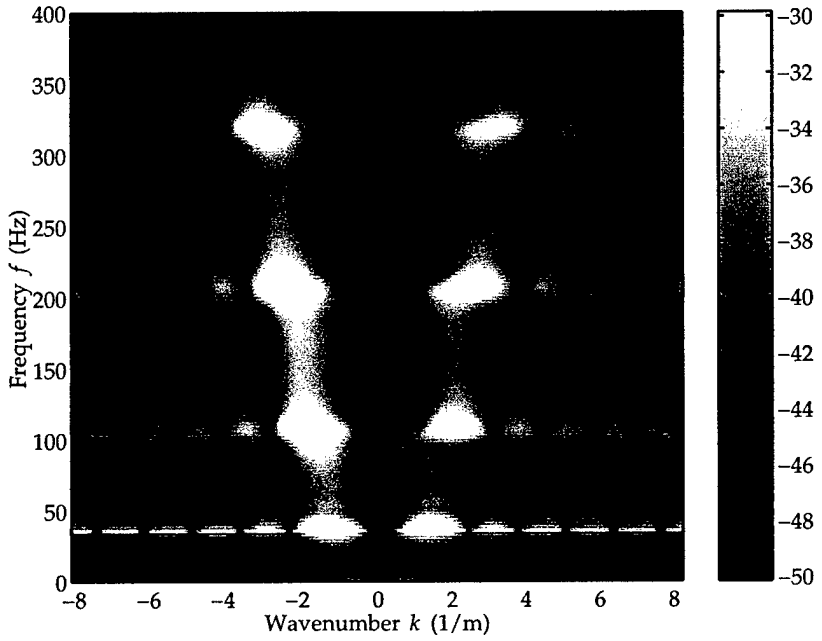

Figure 9: Frequency wavenumber transform of beam acceleration data.

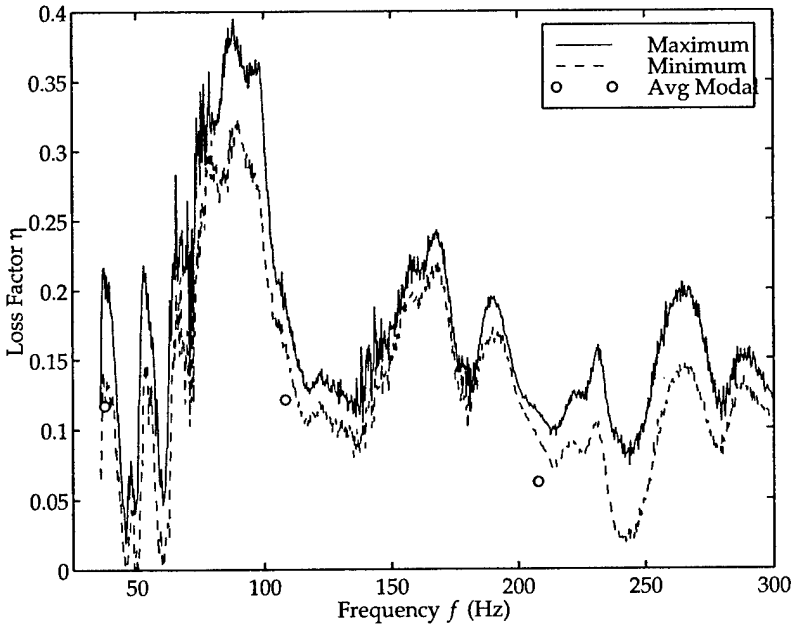

Figure 10: Loss factor versus frequency for four trials: ——, wave envelope maximum; – – –, wave envelope minimum; o o o, modal average.

3.2.2 Loss Factor Estimation

Equations (14)-(16) were used to obtain a wave model estimate of the loss factor. As this model requires nonzero boundary conditions and zero initial conditions, the first 15,000 data points (3 seconds duration) were used for loss factor estimation. For a clear depiction of the variation in loss factor estimates between the four trials considered, the maximum and minimum envelope curves are plotted in Figure 10. Similarly, the maximum and minimum normalized error is plotted in Figure 11. Note that the knee of the error curve occurs at about 225 Hz. Based on the FEM results (recall Figure 3), the wave damping estimates are valid up to this frequency.

As a result, these estimates can be compared to modal estimates obtained using equations (20), (24) and (27) at the first three modal frequencies of 37, 108 and 207 Hz. Since the modal equations apply for homogeneous boundary conditions and nonzero initial conditions, a time window was employed which started after the hammer impact ended. This time corresponds to the first zero crossing of the accelerometer located at $x = 0$. Figure 7 shows this occurs at $t \approx 4$ msec. Data from the 13 accelerometers was used simultaneously in the modal damping estimate. The average modal damping factors are shown in Figure 10. The variation between trials, while not shown, was less than 0.02 for the three modes.

In figure 10, the wave and modal loss factors are seen to be consistent at the three modal frequencies. The average wave model estimate exceeds the average modal estimate by 0.05 for the first two modes and 0.03 for the third mode. In addition, greater variation between

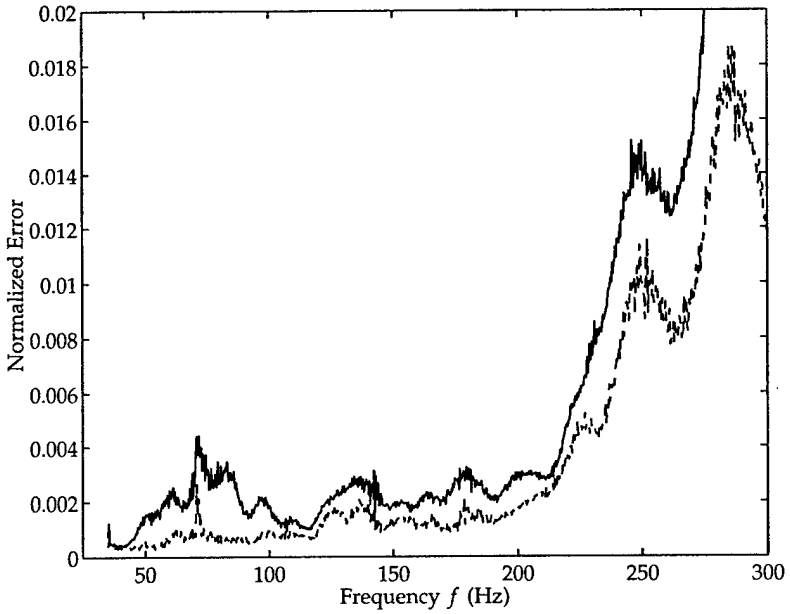

Figure 11: Normalized mean square error versus frequency for four trials: ——, envelope maximum; – – –, envelope minimum.

trials was observed with the wave method.

It is likely that the higher damping estimate obtained by the wave method can be attributed to the difference in data records used with the two methods. Recall that the wave data record must include the time duration of the hammer impact while the modal data record must exclude these data. Thus the modal data window excludes $t \leq 4$ msec shown in Figure 7. While short in comparison to the total temporal record length, note that the omitted acceleration peak at $x = 0$ is five times the value of the first included peak.

It is probable that damping is higher during this initial, high-amplitude time period. This may be due to nonlinear behavior associated with beam bending. Alternatively, starting from rest, the rate of energy absorption by the granular fill may initially exceed its rate of dissipation. From the perspective of the beam's motion, damping would initially be high and decrease until the granular fill reached "steady state" motion in response to forcing by the beam. The inclusion of this early-time data would increase the average damping observed over the time window.

The greater trial-to-trial variation in wave-based loss factor estimation is due to the use of a spatial discretization (13 locations) which is coarse in comparison to the temporal discretization employed in the modal estimate. At the third modal frequency (207 Hz), this corresponds to 4 spatial points per wavelength compared to 20 temporal points per wavelength. A larger number of points per wavelength reduces the effect of sensor noise on the estimate.

4 Conclusions

The wave method compliments traditional modal techniques by making it possible to estimate the loss factor at regularly-spaced frequency values – not just at modal frequencies. The method is applicable for arbitrary forcing applied through the boundary conditions. Furthermore, no specific knowledge of the structure's boundary conditions, material properties or cross-sectional dimensions is required. Since the measurements are Fourier transformed, the data record must be of sufficient duration for the transform to converge. Except when damping depends strongly on amplitude or time, however, this condition is easily met.

The frequency range over which damping can be estimated is limited by several factors. Given a fixed amount of energy at a frequency, the actual loss factor must be large enough to separate wave decay along the length of the beam from signal noise. Thus, there must be sufficient wave energy due to the boundary forcing to produce an acceptable signal to noise ratio. Since realistic forcing is band limited, this condition imposes an upper bound on estimation frequency. Normalized estimation error was found to provide a practical means of determining this upper bound. In addition, when the ratio of wavelength to beam length (λ/L) is large, normalized error is a weak function of loss factor. This imposes a lower bound on estimation frequency. Analysis of numerically and experimentally generated beam data indicates that the first modal frequency ($\lambda/L = 2$) is an adequate lower bound.

5 Acknowledgement

This work was supported by the Office of Naval Research under grant no. N00014-98-1-0755.

References

[1] T. PLONA, B. SINHA, S. KOSTEK and S. CHANG 1992 *The Journal of the Acoustical Society of America* **92**, 1144–1155. Axisymmetric wave propagation in fluid-loaded cylindrical shells. II: Theory versus experiment.

[2] J. VOLLMANN, R. BREU and J. DUAL 1997 *The Journal of the Acoustical Society of America* **102**, 909–920. High-resolution analysis of the complex wave spectrum in a cylindrical shell containing a viscoelastic medium. 2. experimental results versus theory.

[3] J. MCDANIEL, K. LEPAGE and N. MARTIN 1995 *The Journal of the Acoustical Society of America* **98**, 2889. Computation of complex wavenumbers and amplitudes of vibrating structures.

[4] J. PHILLIPS 1996 *Proceedings of the 16th Aerospace Testing Seminar* 355–365. Vibration testing of titan IV-A instrumentation truss with polymeric bead damping.

[5] J. HOUSE 1989 *Polymeric Materials: Science and Engineering, Proceedings of the ACS Division* **60**, 734–738. Damping hollow tubular structures with lightweight visco-elastic spheres.

Evaluation of Granular-fill Damping in Shock Loaded Box Beams

L. Salvino, P. Dupont and J.G. McDaniel, *Proceedings of the 69th Shock and Vibration Symposium*, St. Paul, MN, October 1998.

Proceedings of the 69th Shock and Vibration Symposium, St. Paul, MN, 12-16 October 1998.

Evaluation of Granular-Fill Damping In a Shock-Loaded Box Beam

Liming W. Salvino
Carderock Division, Naval Surface Warfare Center
West Bethesda, MD 20817-5700

Pierre Dupont and J. Gregory McDaniel
Aerospace and Mechanical Engineering, Boston University
Boston, MA 02215

The experimental evaluation of damping performance in a granular-material-filled box beam is presented. The study determined that granular-fill provided significant damping for a high impact excited free-free box beam. A large modal loss factor, exceeding 0.15, was obtained for the few lowest bending modes of the beam. The damping was effective over the frequency range 40 - 300 Hz. A variety of data analyses and modeling methods were used to assess the damping effects from acceleration data. These methods included a novel "complex wave number method" in which the damping values were determined for different wave types over discrete, but regularly-spaced, frequency values. These results were compared with conventional methods such as a modal analysis approach.

INTRODUCTION

The science of granular materials has a long history. Despite its seeming simplicity, granular materials behave differently from the other familiar forms of matter: solids, liquids or gases. One of the unique properties of a granular material, such as a low-density polyethylene bead, is that interactions between bead particles are dissipative due to static fraction and inelastic collisions [1].

While a variety of approaches exist for modifying the damping characteristics of structures constructed from an individual beam, the filling of box beams with granular material has been shown to produce the most significant increase in damping [2]. With proper selection of fill material, such as a bead, significant damping can be achieved with only a modest weight penalty. However, it is clear from existing literature that the mechanism responsible for the damping effectiveness of the granular material differs from that of other more conventional damping treatments.

The work presented in this paper was motivated by the need to determine the dynamic property and damping effectiveness in shock-loaded truss structures composed of many granular material filled box-beams. The damping loss factor[1] associated with each beam may depend on the properties of the fill material, the beam geometry, the load, and their dynamic interactions. This is, in general, difficult to model by analytical methods or numerical simulation. The focus of this work is to determine damping loss factor for a granular material-filled individual beam member when subjected to large impact force excitations. This is achieved by performing experiments and

[1] Damping loss factor η is equal to twice the critical damping ratio at structural resonance.

using the experimental data to assess damping in the frequency range of interest. The knowledge gained from this study should improve the fundamental understanding of structural behavior of a granular-damping-treated beam and provide the basis for further analysis and modeling of a built-up shock loaded truss structure.

APPROACH

A simple experiment was performed to quantitatively assess damping characteristics using a box-beam of typical size in naval applications with two types of granular-materials as damping treatment. The test beam was subjected to hammer impacts at its end. This resulted in average overall peak acceleration levels of the beam in the range of 5 - 50g's. The measured acceleration data were used to determine the damping performance. This included: (1) the determination of shock benefits provided by the damping material and the quantification of those benefits; (2) the determination of the frequency range over which the damping mechanisms is effective (emphasis on frequencies under 300 Hz); and (3) the determination of the relationship between the dynamic g-levels and the measured damping provided by the materials as well as the examination of the energy absorption mechanism for the bead-filled test beam.

Initially, a traditional approach to the analysis of such experimental data sets was used. This may be referred to as a modal approach, where conventional modal parameter estimation and extraction algorithms were employed. The main portions of data analysis were performed using the Complex Exponential Method and Ibrahim Time Domain Method [3]. These algorithms work on measured data in a time domain format, rather than the frequency domain, and extract the damping factor at specific resonant frequencies corresponding to the test specimen. The results of the modal approach can be found in the data analysis section.

A wave model has been developed to analyze the experimental beam data. In this approach, the response along the entire beam at a particular frequency is represented by a fixed number of damped wave types [4]. A brief description of the method is as follows. Based on Euler-Bernoulli theory, a differential equation of a free vibrating beam with no external loads can be written as

$$\rho A\frac{\partial^2 w}{\partial t^2}+\frac{\partial^2}{\partial x^2}\left[EI(x)\frac{\partial^2 w}{\partial x^2}\right]=0 \tag{1}$$

where w is the transverse displacement of any point on the axis of the beam, EI is the flexural rigidity of the beam in the plane of vibrations, and ρA is the mass per unit length of the beam. With a periodic forcing applied at the end of beam, the solution of the above equation is a sum of two forward and two backward propagating waves,

$$w(x,t)=\Re\left\{\sum_{n=1}^{2}F_n e^{i(k_n x-\omega t)}+B_n e^{i[k_n(L-x)-\omega t]}\right\} \tag{2}$$

where $\Re$ refers to the real part. The index n=1,2 refers to flexural and evanescent waves, respectively. The complex wave numbers are

$$k_1=\sqrt[1/4]{\frac{\rho A\omega^2}{EI}} \tag{3}$$

$$k_2=i\sqrt[1/4]{\frac{\rho A\omega^2}{EI}} \tag{4}$$

These wave types can be identified from measured acceleration data shown in the data analysis section. Damping loss factor η is introduced through a complex modulus of elasticity $E(1-i\eta)$.

In addition to the flexural and evanescent waves described above, a box beam also supports plate waves. Each wall of a box beam flexes in and out as plate waves travel down the length of the beam. This type of wave motion can be characterized using Kirchhoff's plate theory. The frequencies of the plate waves for the test beam are above 500 Hz. Since we are focusing on frequencies below 300 Hz, the plate waves were not included in the wave representation of the damping model in this paper.

The key ideas of identifying damping factors by wave model includes several steps. The first step is to convert transient response data in the time domain to independent forced response data at discrete frequency values in the frequency domain using Fast Fourier Transforms (FFT). The next step is to decompose each forced response as a sum of waves and fit the wave field to the measured data. Mean square errors between wave field and data are then minimized by adjusting complex wave numbers. Finally, the damping loss factor η is calculated from the above equations using an error-minimized complex wave number k at each FFT frequency. A complete description of the method can be found in [4].

EXPERIMENTAL ARRANGEMENT

Description of the Box-Beam

A rectangular cross section 10" X 6" X 3/8" box-beam, 16 ft in length, was used in the impact test. The beam weight was estimated to be approximately 603 lbs by calculation. The natural frequencies (in Hz) of the five lowest transverse vibrational (bending) modes for a free-free boundary condition beam are listed in the table below

y X x = 10 X 6	1st mode	2nd mode	3rd mode	4th mode	5th mode
x - x axis	71	194	381	630	941
y - y axis	47	131	256	423	632

The lowest longitudinal and torsional modes of the beam are above 500 Hz, more than 200 Hz above the maximum frequency of interest. Therefore, these modes were ignored in the experimental design and analysis.

Steel plate endcap assemblies, with dimensions of approximately 12" X 8" X 3/4", were bolted to both ends of the beam for convenient installation of fill materials. The two end plates had identical geometrical configurations. The total weight of the beam with endcaps measured 610 lbs.

Fill Material

Shredded Navy tiles (type II, class II) and low-density polyethylene beads (Chevron LDPE 1117B) were used as granular fill material in these tests. The measured bulk density of LDPE beads is 36.8 lbs/ft^3. The volume available to the fill material is 5.40 ft^3. The total weight of the beads needed to fill the beam is approximately 200 lbs. The density of the shredded Navy tile is only slightly larger than that of the beads.

Test Configuration

The test was conducted by suspending the beam horizontally with an elastic cord, approximating free-free boundary conditions. The low-frequency suspension cord was used to ensure that the dynamics of the suspension system would not affect the modal response of the beam. The frequency of this suspension system was estimated to be less than 5 Hz. The suspended beam motion is similar to that of a pendulum. The few possible "rigid body motions" of the pendulum have frequencies estimated to be less than a few Hz. The two transverse directions of the beam were excited separately to obtain the frequencies corresponding to those tabulated in the above table. The excitation forces were generated by an instrumented impact hammer striking at one end of the beam on the side opposite to the acce lerometers. The test configuration is shown in Fig. 1.

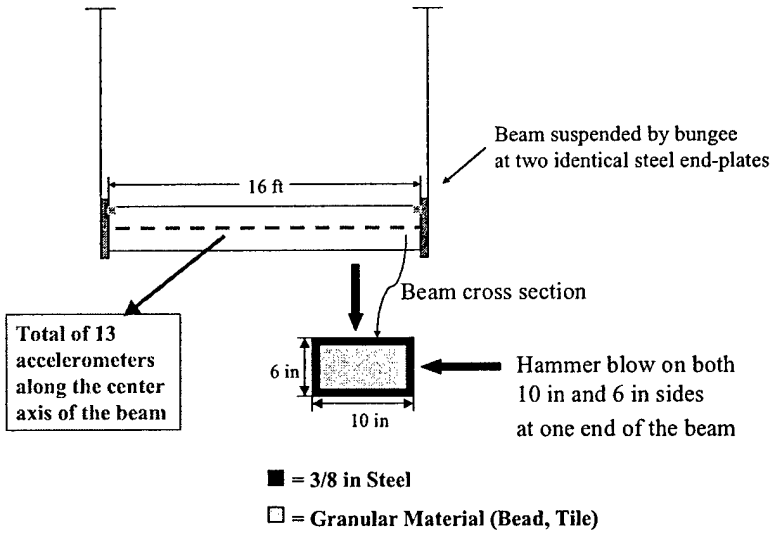

Figure 1. Beam Impact test set-up

Two different hammer tip materials were used during the test. To concentrate the excitations in the lower frequency range, the softer hammer tip was used. The duration of the impulse generated from this material is typically between 15 to 20 milliseconds. These results can be compared to those generated by the harder material tip, which resulted in force pulse duration of approximately 5 to 10 milliseconds. The harder material tip provided energy over a broader frequency range.

A variety of excitation magnitudes were recorded in the test series. It ranged from a few hundred pounds up to 8,000 pounds. The initial peak response acceleration levels were generated from a few g's to above 50 g's. The measured data can be utilized to study the amplitude dependence of the damping.

The test series was conducted on an empty beam to provide the undamped case as a baseline. Two types of granular-fill material, each at the 100% and approximately 80% fill levels were used separately to fill the beam. During the fill process, vibration was applied to the beam (e.g. by hammer tapping) prior to data collection to ensure the granular material was well settled in the beam.

Instrumentation and Data Acquisition

Accelerations at 26 different response locations were measured in transverse directions along two sides of the beam, 13 locations on each side. Accelerometers were spaced approximately 16 inches apart which provided approximately 6 points per wave for the 4th bending mode (400-600 Hz). This arrangement can provide spatial damping performance measurements in addition to temporal measurements.

The uniaxial accelerometers used in the test can measure accelerations up to 50g. The excitation forces at the impact location were also recorded. A data record length of 4 seconds at a sampling rate of 5,000 Hz was stored for each measurement. The final digitized data were stored in ASCII format for analysis and damping evaluation.

DATA ANALYSIS

Beam Time Series Data

The test series was conducted on an empty beam to provide the undamped case as a baseline. Typical accelerometer data comparing empty beam and 100% bead and tile material filled beam is shown in Fig 2.

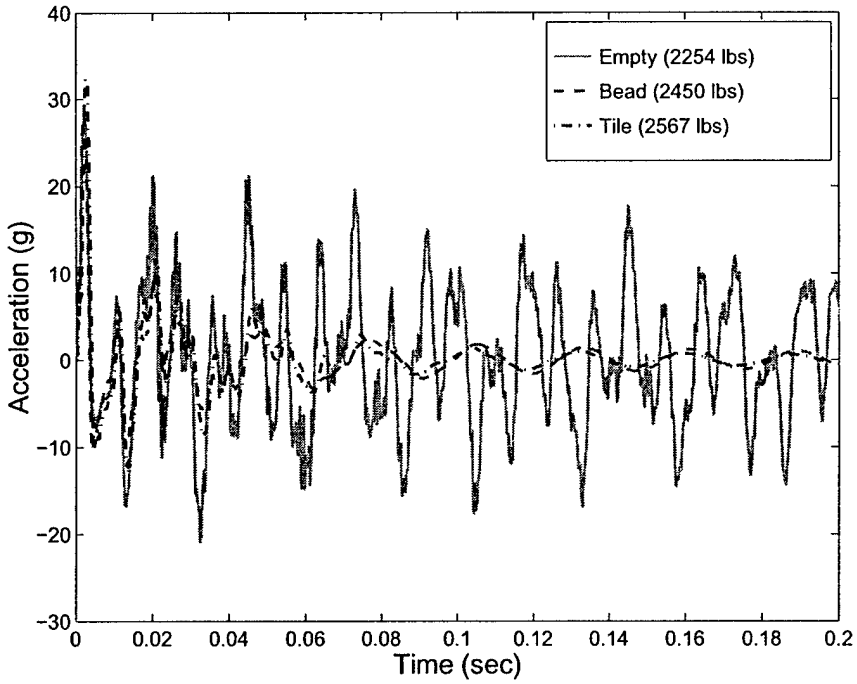

Figure 2. Empty beam is compared with 100% bead- and tile-filled beam. Impact force is approximately 2,400 lbs with pulse duration 10 msec on 10 inch side of the beam. The measured accelerations shown are taken from the nearest channel to the impact point (at x=0).

Modal Characterization of Beam Data

Frequency response functions were calculated using the measured data from the example shown in Fig. 2. These functions were computed using a standard force normalization procedure, namely the measured accelerations were normalized by impact forces with exponential windowing [3]. The frequencies of the lowest three modes for the empty beam were 40.4, 110.2, and 208.1 Hz for excitations on the 10" side (See Fig. 3) and 60.3 163.2, and 310.5 Hz for excitations on the 6" side. The measured frequencies from experimental data were slightly lower compared with the analytical calculations tabulated in previous section. The analytical calculations were done for a free-free beam without end plate.

To check for nonlinearity of the test beam, acceleration measurements were repeated many times using different levels of excitation each time. The amplitude of the frequency response function for the empty beam is independent of excitation forces that ranged from a few hundred pounds to six thousand pounds. The amplitude of the frequency response function for the filled beam (both bead and tile) showed clear variation for the same input force range indicating nonlinearity.

As a means of investigating this nonlinear behavior, a range of impact levels was applied to excite the granular-filled beam in the experiment. Modal estimation and extraction algorithms were then used to determine the damping loss factor for a given impact level. The damping value obtained with this approach, therefore, corresponds to a particular impact level only.

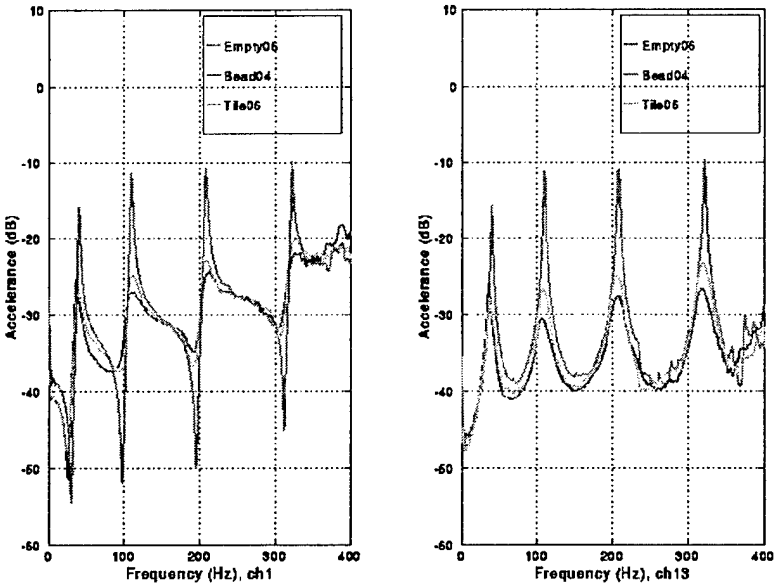

Figure 3. Frequency response function calculated using measured acceleration data normalized by force. Input forces are approximately the same (2,400 lbs) for the empty beam, 100% bead- and tile-filled beam. The plot on the left side corresponds to the measurement closest to the data taken from impact point (x = 0) and the right side corresponds the data taken from the opposite end of the beam (x = L).

A time duration of 500 msec (correspond to 2,500 data points) was used for all damping loss factor calculations, starting at the first zero crossing of the impact point acceleration (taken from the accelerometer located at x=0). Data from all 13 accelerometers were used simultaneously. In Fig. 4, the damping loss factor η is displayed for the empty beam, 100% bead-filled beam and 100% tile filled beam for the lowest two modes corresponding to excitations on the 10" side. The left side of the plot shows higher damping for tile-filled beam compared to the bead-filled beam and damping increases for both types of fill-material with impact force amplitude (the first mode

at 40.4 Hz). The right side of the plot shows higher damping for bead-filled beam compared to the tile-filled beam and damping decreases for both types of fill-material with impact force amplitude (the second mode at 110.2 Hz).

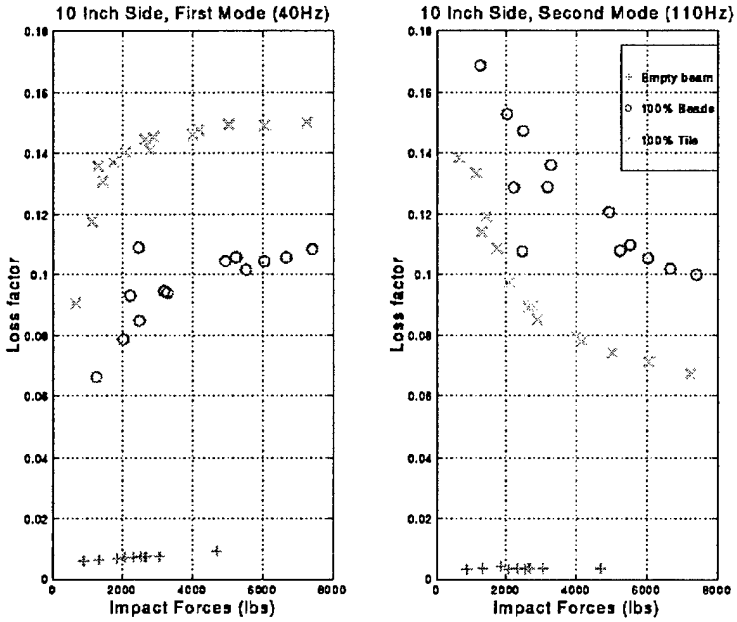

Figure 4. Modal loss factor versus excitation level on 10" side of the beam for empty beam (plus), 100% bead (circle) - and tile (cross) -filled beam. The plot on the left side is for the first mode (at 40.4 Hz) and on the right side is for the second mode (at 110.2 Hz).

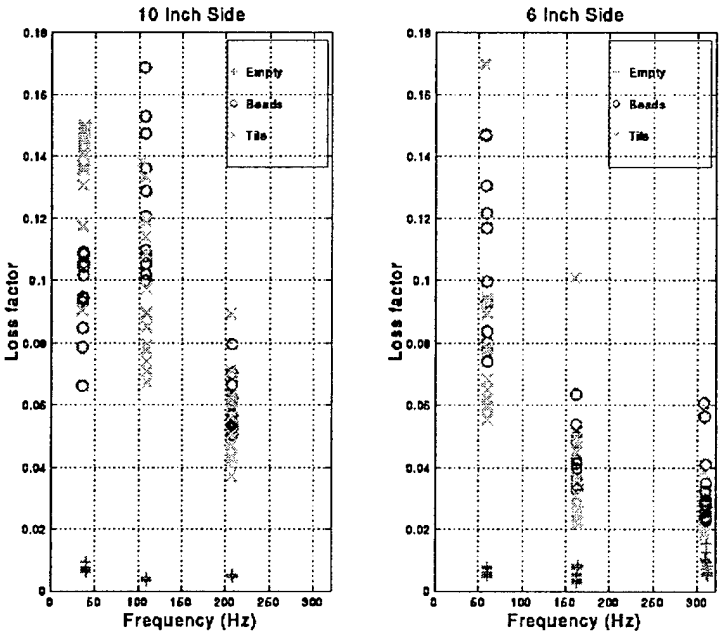

Figure 5. Modal loss factor versus modal frequency for the empty beam (plus), 100% bead (circle) - and tile (cross) -filled beam. The plot on the left side is for excitations on 10" side and on the right side is for excitations on 6" side.

These results strongly indicate that granular-material-damping behavior is a function of response amplitude as well as frequency. To examine the damping performance as a function of frequency, modal loss factors for the empty beam are compared to those for the granular-filled-beam for the three lowest modes on both 10" and 6" sides (Fig. 5). The variation of damping values at particular modal frequencies is primarily due to the different levels of excitation (approximately 600 lbs – 7,000 lbs).

The modal characterization of the granular-material-filled beam indicated that damping exhibits complex dependence on both frequency and amplitude. A more fundamental understanding is needed in order to successfully model this complicated damping behavior. However, the large damping loss factor indicates that the granular damping treatment for box beam under impact load is effective.

Wave Approach

Modeling the frequency-dependent damping behavior from measured data, the wave method was developed to obtain the damping loss factor as a continuous function of frequency. The presence of waves in the measured acceleration data a(x, t) can be verified by taking a two-dimensional Fourier transform

$$A(\omega,k)=\frac{1}{(2\pi)^2}\int_0^T\int_o^L a(x,t)e^{i(kx+\omega t)}dxdt \tag{5}$$

The transform A(ω,k) is maximized whenever the wave number and frequency (k,ω) coincide with that of a natural wave, (k_n,ω_n) as described by

$$a(x,t)=\Re\{A'e^{i(k_n x-\omega_n t)}\} \tag{6}$$

The wave propagation in k-ω plane is given in Fig. 6 .

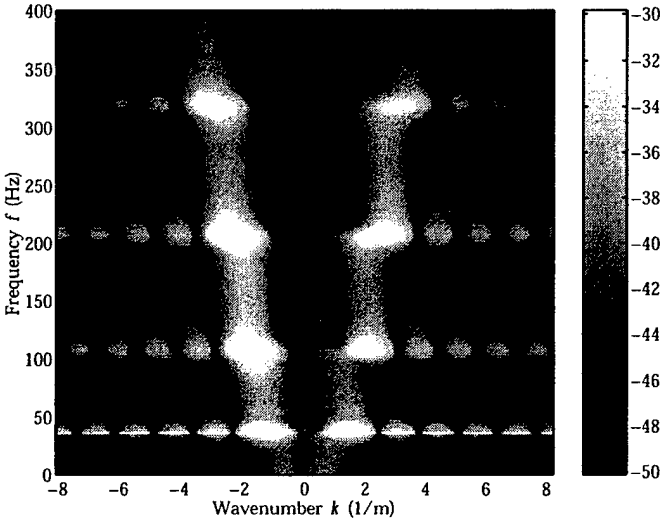

Figure 6. Frequency-wave number transform of acceleration data for the bead-filled beam subjected to a typical impact. The excitation is applied on the 10" side of the beam.

The two branches of the parabola in the k-ω plane are clearly visible in the frequency range $0 \le f \le 300$ Hz. They are particularly strong at the modal frequencies of the beam. The side lobes to the left and right of this parabola are due to the coarse spacing of the sensors (a total of 13 accelerometers). The left branch of the parabola ($k < 0$) corresponds to the wave leaving the impacted end of the beam and the right branch ($k > 0$) corresponds to the wave reflected from the far end. It can be seen that the magnitude of the reflected wave is reduced.

The damping loss factor η can be calculated by the wave model using the procedure described in [4]. Examples of the loss factor η for the bead-filled beam obtained from the wave method are compared with those from several modal methods at the first three modal frequencies in Fig. 7 (excitations on 10" side) and Fig. 8 (excitations on 6" side).

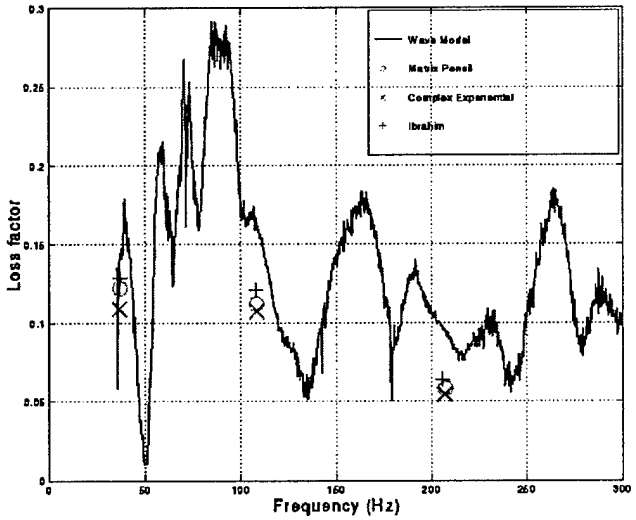

Figure 7.Damp ing loss factor versus frequency for bead-filled beam determined by wave and modal methods. The excitations are on the 10" side of the beam.

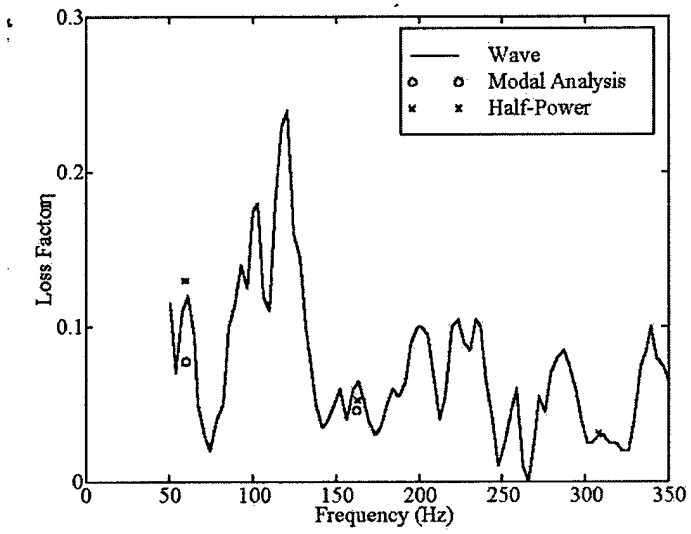

Figure 8.Damp ing loss factor versus frequency for bead-filled beam determined by wave and modal methods. The excitations are on the 6" side of the beam.

Good agreement is observed in Fig. 7 for the first mode and for all modes in Fig. 8, but further investigation is needed to understand the differences for the second and third modes in Fig. 7. Both methods exhibit larger damping for excitations on the 10" side where the beam has lower structural stiffness. A possible explanation is that higher

energy levels can be transferred to the bead-material. Characteristic peaks seen in the wave model suggest that the damping due to granular-fill material is strongly dependent on frequency. The frequency dependent behavior for steady state excitations of a beam has been modeled by others. The average wave model estimate for η exceeds the average modal estimate. It is likely that the difference can be attributed to the difference in the data record length used for the two methods. The reason for this difference in record lengths involves fundamental issues of the two methods. Detailed explanations are given in [4].

SUMMARY

Two distinct approaches were used in the analysis of shock-loaded beam (empty and granular-filled) experimental data. In the conventional modal approach, values of damping loss factors are obtained only for the natural frequencies of the test structure. With the wave model, the damping factor is extracted at each frequency bin of a temporal Fourier transform of the data. The resulting frequency-dependent damping factor can then be applied to predicting the behavior of built-up structures whose modal frequencies do not coincide with those of the test specimen.

Damping benefits provided by granular-material-filled box beam were evaluated and quantified over the frequency range 40 - 300 Hz. These evaluations were carried out for beam transient response data. A variety of impact forces were applied to the test beam, resulting in amplitude- and frequency-dependent damping. Analysis of the test data indicates that granular material provided significant damping for an impact-excited box-beam. The performance of the Type II tile and LDPE beads were comparable, with the tile exhibiting better damping performance at the first mode in some cases. From analysis of the data, the average damping lost factor ranged from $0.06 \leq \eta \leq 0.15$ for the filled beam; for the empty beam, damping loss factor ranged from $0.005 \leq \eta \leq 0.008$. Higher damping was observed for lower structural stiffness under the same excitation forces. In addition, higher damping occurred for lower initial amplitude levels (except for the first mode at 40 Hz) in the range of approximately 7g to 50g. Finally, damping increased with the fill level, that is, the higher the fill level in the beam the better the damping.

ACKNOWDLEGEMENT

The work reported in this paper was funded by the Office of Naval Research. In particular, the authors wish to acknowledge the support of Dr. Geoffrey Main, Dr. Vern Simmons and Mr. William Martin. The technical assistance of J. Rosario, E. Walton, A. Dinsenbacher, William Hay, M. Craun, D. Warwick, D. Feit, and J. O'Brein are also acknowledged.

REFERENCES

[1] Jaeger, H. M., Nagel, S. R., and Behringer, R. P., "Granular solid, liquids, and gases", *Reviews of Modern Physics*, Vol. 68, No. 4, Oct. 1996.

[2] Phillips, J. E. "Vibration testing of titan IV-A instrumentation truss with polymeric bead damping", *Proceedings of the 16th Aerospace Testing Seminar*, pp 355-365, 1996

[3] Ewins, D. J., 1984, *Modal Testing: Theory and Practice*, John Wiley & Sons Inc., New York.

[4] McDaniel, J. G., Dupont, P., and Salvino L. W., "A Wave Approach to Measuring Frequency-dependent Damping Under Transient Loading", submitted to the *Journal of Sound and Vibration,* December, 1998.

Model Reduction Techniques for Shock Loaded Equipment Emulators

P. Dupont and A. Stokes, *Proceedings of the 69th Shock and Vibration Symposium*, St. Paul, MN, October 1998.

69th Shock and Vibration Symposium, St. Paul, MN, 12-16 October 1998.

Model Reduction Techniques for Shock Loaded Equipment Emulators

Pierre Dupont and Ann Stokes
Aerospace and Mechanical Engineering
Boston University
110 Cummington Street
Boston, MA 02215
(617) 353-9596

In a variety of situations, an undesired shock excitation is applied to a master structure that supports shock-sensitive equipment. Often, one wishes to design and test a master structure that transmits the least amount of shock energy to the attached equipment. In scaled testing of new designs, a major task is to design and construct "equipment emulators" – inexpensive mechanical systems which approximately mimic the dynamic behavior of the actual full-scale equipment as seen by the master structure. The method of balanced truncation is presented here as means by which reduced-order equipment emulators with specified error bounds can be designed. The proposed approach uses easily obtainable frequency-domain impedance descriptions of the master structure and actual equipment at the attachment points. The method is illustrated through application to two simple examples.

INTRODUCTION

In recent years, there has been a shift in emphasis from the design of equipment that can withstand high shock loads to the design of structures on which commercial, off the shelf (COTS) equipment can survive. Given the prohibitive cost of testing structural design concepts using full-scale prototypes, finite element models and scaled mechanical models are often employed. In either case, the equipment is typically the most dynamically complex component of the system. Consequently, the construction of detailed numerical or scaled mechanical equipment models can be both difficult and costly. As an alternative, reduced-order equipment models can provide a means of including salient dynamics in the overall model at modest cost. The modeling effort is aided by the fact that the equipment is usually joined to the supporting structure at a small number of attachment points. Thus, the reduced model need only reproduce the input-output behavior at these locations.

The requirements of such a model reduction scheme are as follows. It must be possible to quantitatively characterize the tradeoff between model complexity and modeling error. In particular, modeling error should be expressed by a metric appropriate to the testing goals. For shock qualification, the appropriate metric is the shock spectrum computed from the motion of the master structure at the equipment attachment points. The technique should be based on an "actual" model easily obtained by experiment. Furthermore, the reduced model must be amenable to implementation. For scaled mechanical tests, this means that it must be possible to fabricate the reduced model.

Prior work on the design of scaled mechanical equipment emulators is limited to acoustic performance. Two approaches have been employed in the modeling of equipment cabinets: modal reduction and exact miniaturization. The former consisted of reproducing the first four fixed-base modal frequencies and masses. Design refinement involved adding damping materials to the nominal design to minimize the difference between drive-point impedance of the actual and scaled equipment at the attachment points (considered individually) [1]. The latter method involved the fabrication of a scaled cabinet with a variety of oscillators attached to the shelves [1]. With regard to shock, Barbone and co-workers have developed numerical equipment models, applicable to modally dense systems, which are described by a small number of physically motivated parameters [2,3]. These models have quantifiable error bounds and accurately reproduce early-time relations between forces and displacements at the attachment points. At this time, these techniques have not been evaluated with respect to shock spectrum error, however.

As an alternative to the approaches described above, model reduction can be cast as an optimization problem. Intermediate to solving an optimization problem, balanced truncation provides a simple technique for truncating model states based on their contribution to output energy. For equipment emulation, the output vector is composed of attachment point velocities. The method addresses shock spectrum error indirectly by providing a bound on velocity error energy. The technique and its error bound are described in the following section. Balanced reduction is then applied to two example systems in the subsequent section. Its performance is compared with modal reduction in the time domain as well as in the context of shock spectra. Conclusions are presented in the final section of the paper.

BALANCED TRUNCATION

As in [1,2,3], it is assumed that the input-output behavior of the equipment at its attachment points can be represented using a linear model. If the equipment is attached to the structure by a shock or vibration mount, this implies the use of an above-mount equipment model. The use of linear models is also motivated by the observation that scaled testing is often conducted using nondestructive input amplitudes to allow for repeated trials. With this assumption, the equipment can be expressed as a first-order state space system given by

$$\dot{x}(t) = Ax(t) + bu(t), \quad y(t) = Cx(t) \tag{1}$$

where $u \in R^M$ is a vector of inputs (attachment point forces), and $y \in R^M$ is a vector of outputs (attachment point velocities). The vector $x \in R^N$ is referred to as the state vector, which consists of displacement and velocity quantities for a discretized model of the emulator. The number of attachment points is far fewer than the number of degrees of freedom of the model, so that $M << N$. The input-output transfer function $y(s)=G(s)u(s)$ associated with (1) is

$$G(s) = C(sI - A)^{-1}B \tag{2}$$

which can be obtained experimentally from measurements of drive-point and transfer admittance. The triplet of matrices (A, B, C) is called a realization of $G(s)$. While the transfer function is unique, the realization is not. If T is an invertible matrix, then the triple (TAT^{-1}, TB, CT^{-1}) is another realization. The goal of model reduction is to solve for an approximate model $\hat{G}(s)$ possessing $L < N$ system states while introducing the least error in the transfer function $G(s)$. Error can be described by $\left\|G(s) - \hat{G}(s)\right\|$ where $\|\cdot\|$ is an induced matrix norm.

In the field of structural dynamics, modal realizations are often employed in model reduction. For a modal realization, TAT^{-1} is block diagonal, so that

$$TAT^{-1} = \mathrm{diag}\left(\begin{bmatrix} -\zeta_1\omega_1 & -\sqrt{1-\zeta_1^2}\,\omega_1 \\ \sqrt{1-\zeta_1^2}\,\omega_1 & -\zeta_1\omega_1 \end{bmatrix}, \ldots, \begin{bmatrix} -\zeta_{N/2}\omega_{N/2} & -\sqrt{1-\zeta_{N/2}^2}\,\omega_{N/2} \\ \sqrt{1-\zeta_{N/2}^2}\,\omega_{N/2} & -\zeta_{N/2}\omega_{N/2} \end{bmatrix}\right) \tag{3}$$

Each 2×2 submatrix corresponds to a pair of the N system states. In modal truncation, pairs of states are eliminated from the model based on a criteria such as rate of decay, $\zeta_i\omega_i$, frequency, $\sqrt{1-\zeta_i^2}\,\omega_i$, or transfer function error. The latter quantity is given by $\|C_iB_i\|/|\zeta_i\omega_i|$ [6]. Transfer function error is the most appropriate of these for equipment model reduction. Modal truncation has the advantage of being conceptually simple. In addition, it provides a physical interpretation of the system states as modes. The technique can become impractical, however, when a structure possesses many modes whose contributions to the transfer function error are comparable. This is true of modally dense systems, such as COTS equipment cabinets [1].

Given the goal of model reduction, truncation should ideally be performed on the realization in which the retained states minimize the error norm, $\left\|G(s) - \hat{G}(s)\right\|$. Clearly, this optimal choice of realization will depend both on $G(s)$ and on the number of states to be retained, L. Furthermore, there is no reason to assume that a modal realization is

close to the optimal. In contrast, a balanced realization is one in which the states are selected according to input-output energy transfer. Those states least involved in energy transfer are truncated. While not optimal, it is shown below that this method provides excellent approximation of modally dense structures.

A description of a balanced realization for the transfer function $G(s)$ requires the introduction of the controllability gramian P and observability gramian Q. These gramians satisfy the equations:

$$\begin{aligned} AP+PA^T+BB^T&=0\\ A^TQ+QA+C^TC&=0 \end{aligned} \tag{4}$$

The observability gramian has the interpretation (see, e.g., [4]) offered by the following calculation. Given the input $u(t)=0,\ t>0$ and initial state $x(0)=x_0$, then $\int_0^\infty y(t)^T y(t)=x_0^TQx_0$. If Q has certain very small eigenvalues, then the initial conditions corresponding to those eigenvectors will have very little effect upon the output. The controllability gramian can be interpreted by calculating the minimum control energy which was needed to move the state vector x from the origin to its initial value $x(0)=x_0$. Mathematically, this can be posed as the following optimization problem. Find $J(u_{opt})=\min_{u\in L_2(-\infty,0)}\int_{-\infty}^0 u^T(t)u(t)dt$ subject to (1) and $x(0)=x_0$. The solution is given by $J(u_{opt})=x_0^TP^{-1}x_0$ [6]. Thus, if certain eigenvalues of P are very small, then the states $x(0)$ associated with those eigenvalues are very difficult (control costly) to achieve. Assuming $u(t)=0,\ t>0$, these results can be combined to yield the ratio of future output energy to prior minimum input energy associated with an arbitrary initial state, x_0 [6].

$$\sup_u \frac{\int_0^\infty y(t)^T y(t)}{\int_0^\infty u(t)^T u(t)}=\frac{x_0^TQx_0}{x_0^TP^{-1}x_0}=\frac{w^TP^{1/2}QP^{1/2}w}{w^Tw},\quad x_0=P^{1/2}w \tag{5}$$

The eigenvalues of $P^{1/2}QP^{1/2}$ can be seen to provide a means of ranking the importance of state space directions (described by eigenvectors) in terms of their 2-norm contribution to this energy. Consequently, a realization that diagonalizes $P^{1/2}QP^{1/2}$ makes it possible to apply this ranking directly to the realization's states.

Such a realization $(\overline{A},\overline{B},\overline{C})$ is termed balanced and can be shown to satisfy

$$\begin{aligned} \overline{A}\Sigma+\Sigma\overline{A}^T+\overline{B}\overline{B}^T&=0\\ \overline{A}^T\Sigma+\Sigma\overline{A}+\overline{C}^T\overline{C}&=0 \end{aligned} \tag{6}$$

The observability gramian and controllability gramians in this case are identical, diagonal matrices $\Sigma=\mathrm{diag}(\sigma_1,\sigma_2,\ldots\sigma_N),\ \sigma_i>0$. The realization is termed ordered if $\sigma_1>\sigma_2>.\sigma_N$.

Any asymptotically stable, minimal realization (A,B,C) with observability gramian Q and controllability gramian P can be transformed into a balanced realization (TAT^{-1},TB,CT^{-1}) where $P=RR^T$ is a Cholesky factorization of P, $RQR^T=U\Sigma^2U^T$ is a singular value decomposition of RQR^T, and $T=\Sigma^{1/2}U^TR^{-1}$ [6]. The truncation of a balanced realization results in a stable, minimal system. Let $(\overline{A},\overline{B},\overline{C})$ be an ordered, balanced realization with transfer function $G(s)$. The diagonal gramian Σ is partitioned as $\Sigma=\mathrm{diag}(\Sigma_1,\Sigma_2)$, where $\Sigma_2=\mathrm{diag}(\sigma_{L+1},\sigma_2,\ldots\sigma_N)$ consists of "small" elements. The matrices $(\overline{A},\overline{B},\overline{C})$ are partitioned conformably, so that

$$\overline{A}=\begin{pmatrix}A_{11}&A_{12}\\A_{21}&A_{22}\end{pmatrix},\quad \overline{B}=\begin{pmatrix}B_1\\B_2\end{pmatrix},\quad \overline{C}=\begin{pmatrix}C_1&C_2\end{pmatrix} \tag{7}$$

The truncated system (A_{11}, B_1, C_1) is stable, with transfer function $\hat{G}(s)$. The approximation satisfies the bound [6]

$$\left\| G(s) - \hat{G}(s) \right\|_\infty \leq 2 \sum_{i=L+1}^{N} \sigma_i \tag{8}$$

where the infinity norm for the system $y(s) = G(s)u(s)$ is defined by

$$\left\| G(s) \right\|_\infty = \sup_u \frac{\int_0^\infty y(t)^T y(t)}{\int_0^\infty u(t)^T u(t)} \tag{9}$$

One technical difficulty with the technique described above is that if $G(s)$ is a passive transfer function (i.e., it does not produce energy) then $\hat{G}(s)$ is not necessarily passive. Mathematically the passivity condition is given by $G(i\omega) + G^*(i\omega) \geq 0$ or, for single-input single-output systems, the phase must be less than $\pm 90^\circ$). This technical point turns out to be very important since it is desired to fabricate equipment models using passive mechanical elements. The issue can be resolved with a method of passivity preserving balanced truncation described in [5]. The performance (both theoretically and in practice) is not compromised by the modified technique. The approach is illustrated below for two example systems.

EXAMPLE 1

A single-input single-output system was used to compare the performance obtained through balanced and modal truncation. The system is depicted in Fig. 1. An equipment model possessing 36 modes (72 states) is attached to a master structure with a fixed-base frequency normalized to unity. The equipment modes possess a uniform random frequency distribution in the interval [0.6,1.4]. Their magnitudes correspond to a uniform distribution in the interval [0,1]. This equipment model was selected to reflect the ambiguity encountered when attempting a modal reduction of equipment possessing moderate modal density.

Using the attachment point force and velocity as the input and output, respectively, the equipment model was reduced to four modes (8 states) using balanced and modal truncation. (The latter was carried out using $\left\| C_i B_i \right\| / \left| \zeta_i \omega_i \right|$ to rank the contribution of each mode to transfer function error.) With this choice of input and output, the transfer function corresponds to mechanical admittance. The admittance magnitude for the entire system (equipment and master structure) is plotted in Fig. 2. This quantity can be interpreted as the response of the master structure to a vertical disturbance force. From this plot, it can be seen that balanced truncation provides a better match to the full system in the neighborhood of the master structure's fixed-base frequency. While not depicted, this is also true of admittance phase angle. Furthermore, balanced truncation provides better low and high frequency amplitude matching.

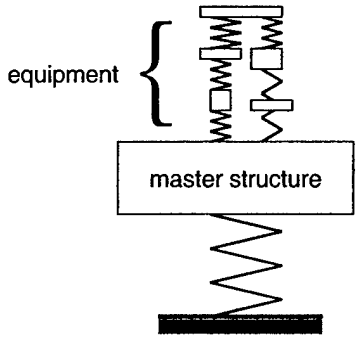

Fig. 1. One dimensional example system. The equipment model has 36 modes (72 states) uniformly distributed about the fixed-base frequency of the master structure.

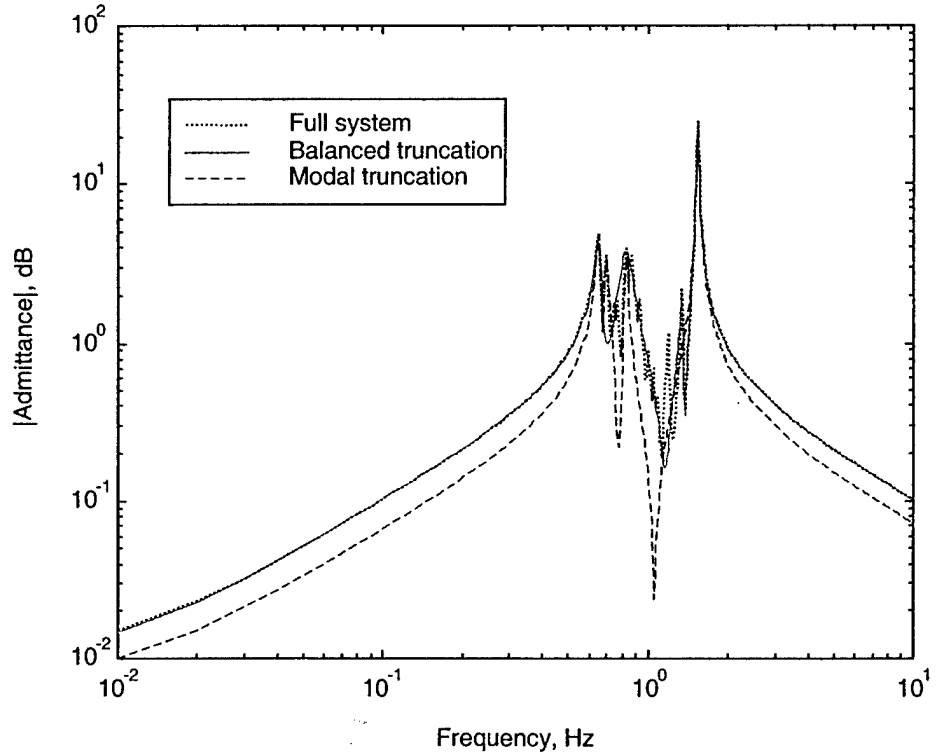

Fig. 2. Admittance (velocity/force) magnitude plots for systems consisting of the master structure and the full, balanced or modal equipment models.

To compare the truncation techniques in terms of shock severity, the shock spectrum of the master structure was computed in response to a half-sine force pulse of duration 0.5 seconds. The result is shown in Fig. 3. It can be seen that the modal truncation model causes the shock spectrum to be underestimated in the neighborhood of the master structure's fixed-base frequency by a factor of 0.52 to 0.67. This indicates that the modally truncated system absorbs significantly more energy in this frequency range than does the actual equipment. To a lesser degree, this model also underpredicts the shock spectrum at high frequencies. A shock trial conducted with such a model would erroneously suggest that the master structure provides a much safer shock environment than in actuality. In contrast, the equipment model obtained by balanced truncation provides good shock spectrum matching over the entire frequency range.

EXAMPLE 2

A two-dimensional finite element cabinet model was developed in order to test the passive, balanced realization technique for structures of more realistic complexity. The cabinet is constructed of beam elements and consists of three main compartments, with stringers and masses intended to simulate internally mounted components. The model appears in Fig. 4. There are two inputs and two outputs consisting of the vertical forces and velocities, respectively, measured at drive points 1 and 2. The stringer stiffnesses and masses were randomly chosen, so that a number of modes involving motion of the stringers and cabinet structure lie in the range of 15-40 Hz.

The full finite element model of the cabinet has 24 states, which through passive balanced truncation, is reduced to 4. The two drive point admittance magnitudes (diagonal elements of $G(s)$) are shown in Fig. 5 and Fig. 6. As was the case for the one-dimensional example, both low and high frequency asymptotic behavior is well captured by the truncation. In addition, the major dynamic effects are captured for all intermediate frequencies.

To confirm these observations, the cabinet model was mounted on a master structure consisting of a simply supported beam. The beam properties were chosen such that the modal frequencies and admittance amplitudes were

comparable to those of the cabinet at the attachment points. The velocity response of the combined system to an impulsive force applied at attachment point 1 is shown in Fig. 7. The system incorporating the truncated equipment model accurately predicts both early and late time response. The shock spectrum at attachment point 1 of the combined system is plotted in Fig. 8 for a half-sine force pulse applied at this point. Excellent agreement between the full and reduced systems is observed.

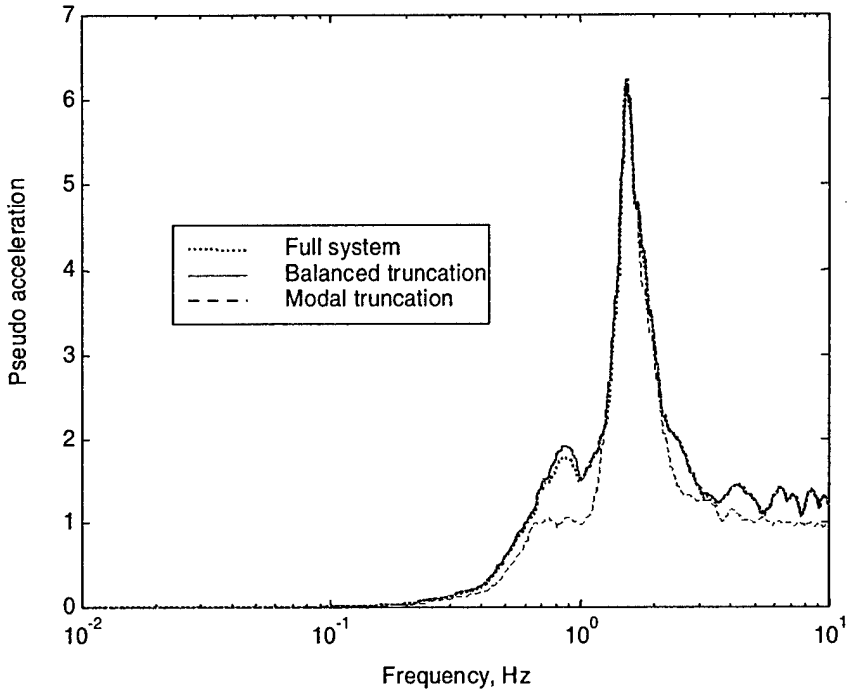

Fig. 3. Shock spectrum with 5% damping comparing response of the master structure to a half-sine force pulse for the full and truncated equipment models.

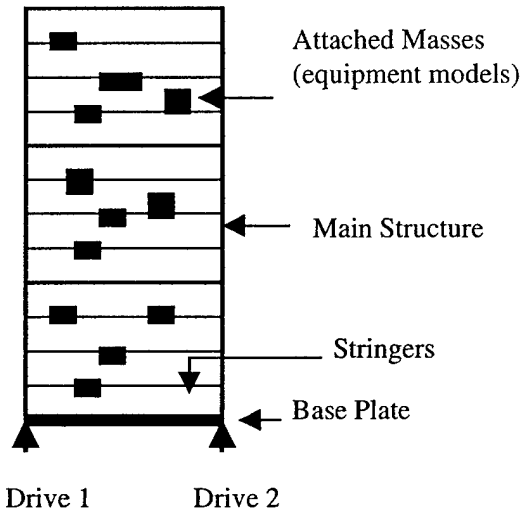

Fig. 4. Two-dimensional cabinet model. The two inputs and two outputs consist of the vertical drive point forces and velocities, respectively.

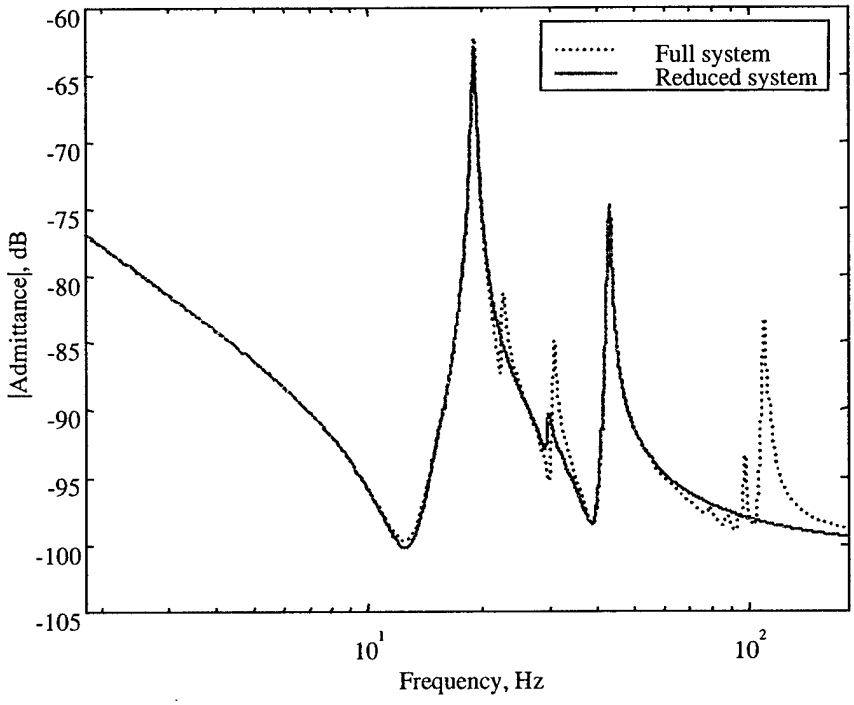

Fig. 5. Drive point admittance (velocity/force) at attachment point 1 for the full-order and reduced-order systems.

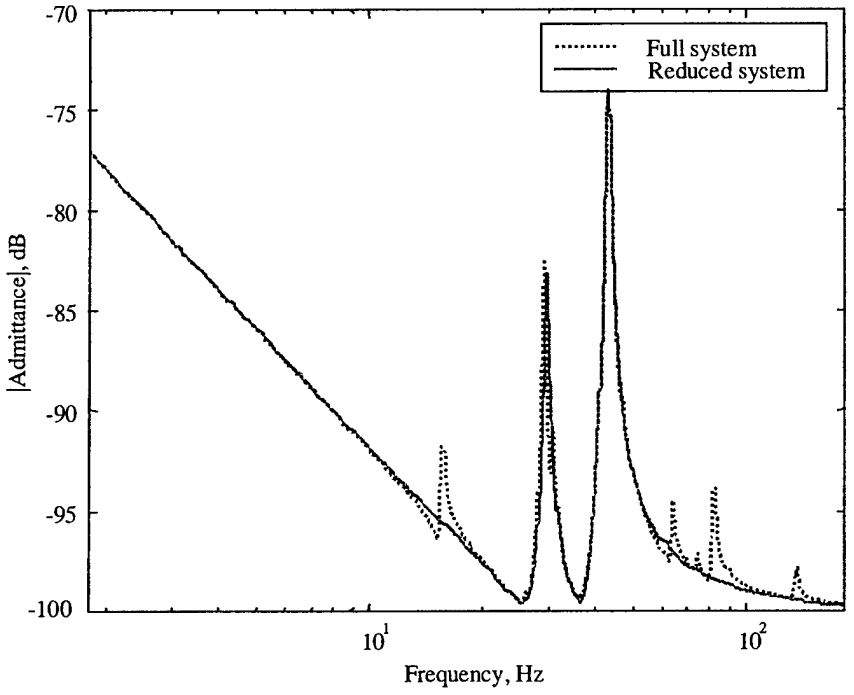

Fig. 6. Drive point admittance (velocity/force) at attachment point 2 for the full-order and reduced-order systems.

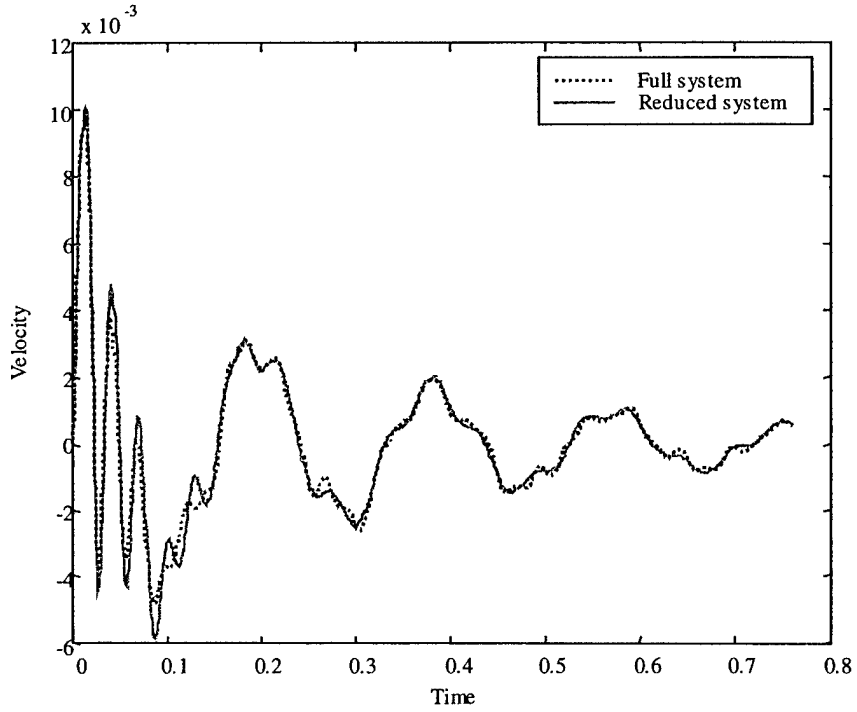

Fig. 7. Deck velocity at attachment point 1 in response to an impulsive force input.

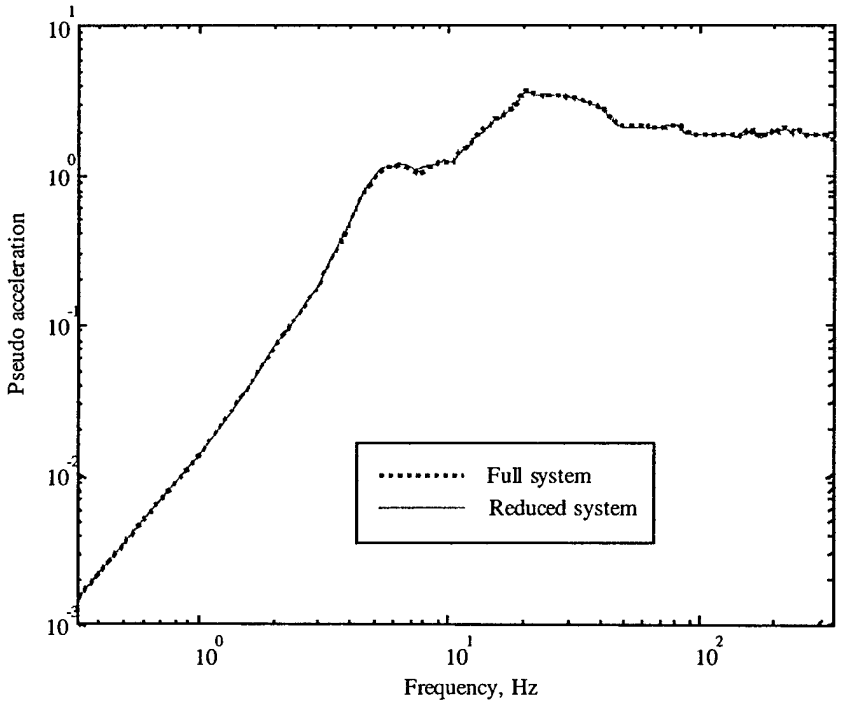

Fig. 8. Shock spectrum (5% damping) at attachment point 1 for the full-order and reduced-order systems.

CONCLUSIONS

Balanced truncation has been demonstrated as an effective alternative to modal truncation for the design of numerical or scaled mechanical equipment models. The method is inspired by the desire to minimize input-output error energy described in terms of 2-norms. The relationship between model complexity and error energy can be ascertained using known error bounds that depend on the truncated states. A simple modification makes it possible to ensure that the reduced system preserves the passivity of the full-order model.

The application of the approach to two example systems indicates that balanced truncation is effective from the viewpoints of the time, frequency and shock spectra domains. In addition, the first example established that balanced truncation may be superior to modal truncation in the context of shock loading. Additional work is needed to fully understand the analytical and practical implications for the emulation of actual equipment. Furthermore, for multi-input multi-output systems, no systematic technique exists for fabricating a reduced model obtained either through modal or balanced truncation. These issues are topics of current study.

ACKNOWLEDGEMENTS

We gratefully acknowledge the support of ONR through Dr. Geoffrey Main.

REFERENCES

1. Haberman, R., 1995, "Frequency Response Characteristics of Electrical Cabinets and Scale Model Simulators," BBN Technical Memorandum No. NL-471.
2. Cherukuri, A. and Barbone, P., "High Modal Density Approximations for Equipment in the Time Domain," *Journal of the Acoustical Society of America*, 1998, Vol. 104, No. 4, pp. 2048-2053.
3. Barbone, P., Cherukuri, A. and Goldman, D., "Canonical Representations of Complex Vibratory Subsystems: Time Domain Dirichlet to Neumann Maps," *International Journal of Solids and Structures*, 1999, in press.
4. K. Glover, "All Optimal Hankel-norm Approximations of Linear Multivariable Systems and Their L^{∞} Bounds," *International Journal of Control*, 1984, Vol. 39, No. 6, pp. 1115-1193.
5. Chen, X., and Wen, J., "Positive Realness Preserving Model Reduction with H_{∞} Norm Error Bounds", *IEEE Transactions on Circuits and Systems-1 Fundamental Theory and Applications*, 1995, Vol. 42, No. 1, pp. 23-29.
6. Green, M. and D.J.N. Limebeer, 1995. **Linear Robust Control** , Prentice Hall, Englewood Cliffs, NJ.
7. Zhou, K., 1996, **Robust and Optimal Control,** Prentice Hall, Englewood Cliffs, NJ.

An Error Measure for the Shock Testing of Scale Models

P. Dupont and J.G. McDaniel, 16th International Conference on Acoustics and 135th Meeting of the Acoustical Society of America, Seattle, WA, June 1998

16th International Congress on Acoustics and 135th Meeting Acoustical Society of America, Seattle, 20-26 June 1998.

AN ERROR MEASURE FOR THE SHOCK TESTING OF SCALE MODELS

Pierre Dupont and J. Gregory McDaniel

Aerospace and Mechanical Engineering, Boston University, Boston, MA 02215

Abstract: In a variety of situations, an undesired shock excitation is applied to a master structure that supports shock-sensitive equipment. Often, one wishes to design and test a master structure that transmits the least amount of shock energy to the attached equipment. In scaled testing of new designs, a major task is to design and construct "equipment emulators" – inexpensive mechanical systems which approximately mimic the dynamic behavior of the actual full-scale equipment as seen by the master structure. A new method is presented for assessing the fidelity of equipment emulators and for interpreting test data taken in the presence of imperfect emulators. The proposed approach uses easily obtainable frequency-domain impedance descriptions of the master structure and actual equipment at the attachment points. These ideas may provide a path by which experimentalists can efficiently arrive at conceptual designs of emulators that promise a specified degree of fidelity in terms of attachment point velocities and their associated shock spectra. The ideas are illustrated by application to the emulation of commercial-grade electronic cabinets for the testing of novel ship deck structures.

INTRODUCTION

In the design and use of scale equipment models for shock testing, there are two principal objectives. The first is to produce conceptual mechanical designs that satisfy specified error and cost/complexity criteria. Given a mechanical emulator, the second objective is to develop post-processing techniques that account for emulation error in the interpretation of shock trial data.

Prior work on the design of mechanical equipment emulators is limited to acoustic performance. The design approach consisted of reproducing the first four fixed-base equipment modal frequencies and masses. Design refinement involved adding damping materials to the nominal design so as to minimize the difference between drive-point impedance of the actual and scaled equipment at the attachment-points (1). With regard to shock, Barbone is developing numerical equipment models, described by a small number of physically motivated parameters, that reproduce early-time relations between forces and displacements at the attachment points (2).

In both approaches, a physical understanding is employed to obtain a simplified model of an otherwise highly complex dynamic system. The modeling is performed independent of the dynamics of the master structure. And while the latter approach directly addresses error criteria during modeling, neither provides a means to post-process experimental data to account for emulation error. A significant issue is the lack of a generally accepted definition for emulation error in the context of shock loading and an easily evaluated metric for assessing this error. The contribution of this paper is to propose such a measure.

EMULATOR ERROR

Emulator error is evaluated in the context of the scaled master structure. It is defined as the vector difference between attachment-point velocities obtained with a particular emulator and those that would be obtained with perfectly scaled equipment. It can be expressed as a transfer function matrix relating measured scale model velocities to the velocity error vector. As a metric of emulation error, the maximum and minimum singular values of the transfer function matrix can be plotted as a function of frequency. These values represent the maximum and minimum gains for all possible attachment-point velocity vectors. By taking appropriate norms of a related transfer function, emulation error can also be expressed in terms of shock spectrum bounds. Using the proposed transfer functions, experimental data can be corrected for emulator error. Using norms, experimental shock spectrum error can be bounded.

As a simple illustration of this method, Figure 1 depicts an equipment cabinet mounted on a master structure consisting of a simply supported beam. Considering only vertical motion, an analytical model of the beam, together with experimental data from actual and scale model cabinets, is employed. Comparison between drive-point impedance of the actual and emulated cabinets in Figure 2 suggests minimal error from 0-200 Hz and large errors outside that range. In contrast, the singular values of the 2×2 velocity error transfer function matrix shown in

Figure 3 indicate significant error from 0-400 Hz and small error from 420-700 Hz. Note also the effect of master structure impedance on error. Roughly speaking, a modest error is amplified (attenuated) when stringer impedance is small (large). The proposed method offers the advantages of: (i) ease of application, (ii) error evaluation in the context of the master structure, and (iii) a means for considering all possible attachment-point velocities.

ACKNOWLEDGEMENTS

We gratefully acknowledge the support of ONR through Dr. Geoffrey Main. We thank Robert Haberman of BBN for making the cabinet data available to us.

REFERENCES

1. Haberman, R., "Frequency Response Characteristics of Electrical Cabinets and Scale Model Simulators," BBN Technical Memorandum No. NL-471, 1995.
2. Cherukuri, A. and Barbone, P., "High Modal Density Approximations for Equipment in the Time Domain," *Journal of the Acoustical Society of America*, in press, 1998.

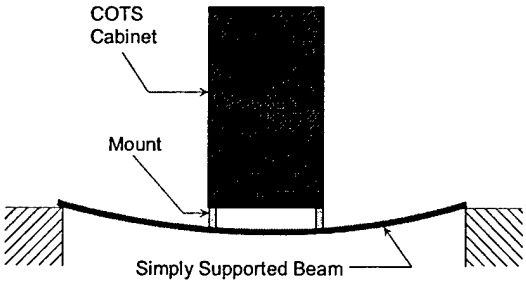

FIGURE 1. Equipment cabinet mounted on beam.

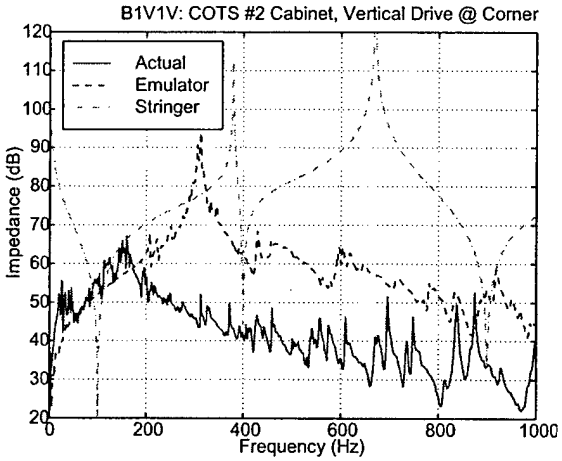

FIGURE 2. Vertical drive point impedance of cabinet, emulator and stringer (beam).

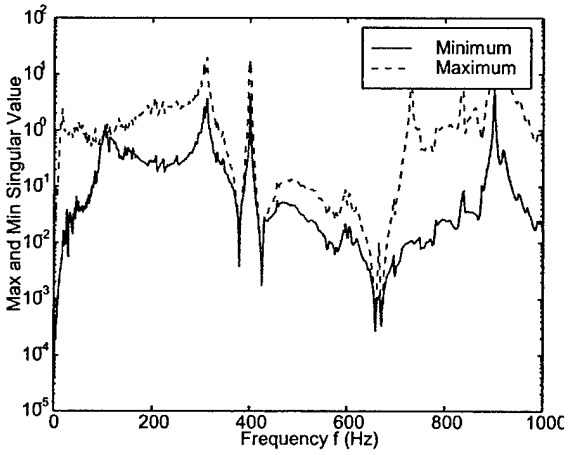

FIGURE 3. Maximum and minimum singular values of transfer function matrix relating measured vertical attachment point velocity to velocity error.